Cell Reports

RNA helicase IGHMBP2 regulates THO complex to ensure cellular mRNA homeostasis

Graphical abstract

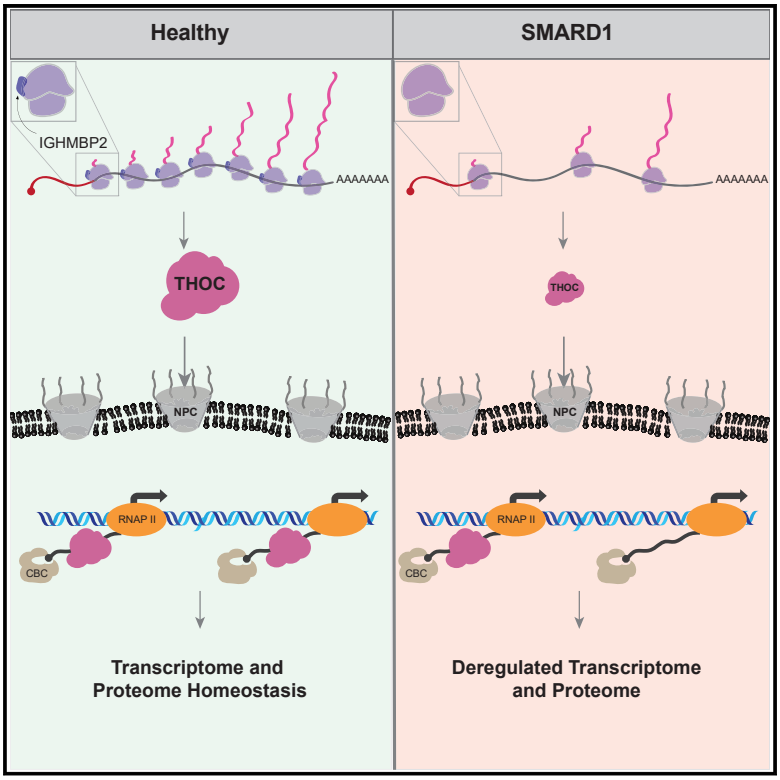

Highlights

- C-terminus of the RNA helicase IGHMBP2 binds 80S ribosomes
- IGHMBP2 aids translation of short, GC-rich 5′ UTR mRNAs
- Loss of IGHMBP2 results in THOC downregulation
- Deregulated mRNA metabolism likely contributes to SMARD1 disease

Authors

Archana Bairavasundaram Prusty, Anja Hirmer, Julieth Andrea Sierra-Delgado, ..., Sibylle Jablonka, Florian Erhard, Utz Fischer

Correspondence

archana.prusty@uni-wuerzburg.de (A.B.P.), florian.erhard@informatik.uni-regensburg.de (F.E.), utz.fischer@uni-wuerzburg.de (U.F.)

In brief

Prusty et al. demonstrate that IGHMBP2 aids in the translation of a small subset of transcripts, including TREX components THOC1 and THOC2, to ensure cellular transcriptome homeostasis. The deregulation of transcriptome and proteome upon IGHMBP2 loss of function might contribute to the etiology of SMARD1 disease.

Prusty et al., 2024, Cell Reports *43*, 113802
February 27, 2024
https://doi.org/10.1016/j.celrep.2024.113802

Cell Reports

CellPress
OPEN ACCESS

Report

RNA helicase IGHMBP2 regulates THO complex to ensure cellular mRNA homeostasis

Archana Bairavasundaram Prusty,[1,*] Anja Hirmer,[1] Julieth Andrea Sierra-Delgado,[2] Hannes Huber,[1] Ulf-Peter Guenther,[3] Andreas Schlosser,[4] Olexandr Dybkov,[5] Ezgi Yildirim,[6] Henning Urlaub,[5,7,8,9] Kathrin C. Meyer,[2,10] Sibylle Jablonka,[6] Florian Erhard,[11,12,*] and Utz Fischer[1,13,14,*]

[1]Department of Biochemistry 1, Biocenter, University of Würzburg, 97074 Würzburg, Germany
[2]Nationwide Children's Hospital, Center for Gene Therapy, Columbus, OH 43205, USA
[3]DKMS Life Science Lab gGmbH, 01069 Dresden, Germany
[4]Rudolf-Virchow-Center, Center for Integrative and Translational Bioimaging, University of Würzburg, 97080 Würzburg, Germany
[5]Bioanalytical Mass Spectrometry, Max Planck Institute for Multidisciplinary Sciences, 37077 Göttingen, Germany
[6]Institute of Clinical Neurobiology, University Hospital Würzburg, 97078 Würzburg, Germany
[7]Department of Clinical Chemistry, University Medical Center Göttingen, 37075 Göttingen, Germany
[8]Cluster of Excellence "Multiscale Bioimaging: from Molecular Machines to Networks of Excitable Cells" (MBExC), University of Göttingen, Göttingen, Germany
[9]Göttingen Center for Molecular Biosciences, University of Göttingen, Göttingen, Germany
[10]Department of Pediatrics, Ohio State University, Columbus, OH 43210, USA
[11]Institute for Virology and Immunobiology, University of Würzburg, 97078 Würzburg, Germany
[12]Faculty for Informatics and Data Science, University of Regensburg, 93053 Regensburg, Germany
[13]Helmholtz Institute for RNA-based Infection Research (HIRI), Helmholtz Centre for Infection Research (HZI), 97080 Würzburg, Germany
[14]Lead contact
*Correspondence: archana.prusty@uni-wuerzburg.de (A.B.P.), florian.erhard@informatik.uni-regensburg.de (F.E.), utz.fischer@uni-wuerzburg.de (U.F.)
https://doi.org/10.1016/j.celrep.2024.113802

SUMMARY

RNA helicases constitute a large protein family implicated in cellular RNA homeostasis and disease development. Here, we show that the RNA helicase IGHMBP2, linked to the neuromuscular disorder spinal muscular atrophy with respiratory distress type 1 (SMARD1), associates with polysomes and impacts translation of mRNAs containing short, GC-rich, and structured 5′ UTRs. The absence of IGHMBP2 causes ribosome stalling at the start codon of target mRNAs, leading to reduced translation efficiency. The main mRNA targets of IGHMBP2-mediated regulation encode for components of the THO complex (THOC), linking IGHMBP2 to mRNA production and nuclear export. Accordingly, failure of IGHMBP2 regulation of THOC causes perturbations of the transcriptome and its encoded proteome, and ablation of THOC subunits phenocopies these changes. Thus, IGHMBP2 is an upstream regulator of THOC. Of note, IGHMBP2-dependent regulation of THOC is also observed in astrocytes derived from patients with SMARD1 disease, suggesting that deregulated mRNA metabolism contributes to SMARD1 etiology and may enable alternative therapeutic avenues.

INTRODUCTION

Eukaryotic cells determine the final protein output of their genetic program not only at the transcriptional level but also post-transcriptionally, by regulating localization, translation, and turnover rates of their mRNAs. Ultimately, the coding potential of any mRNA is determined by the ensemble of all associated RNA-binding proteins (RBPs), non-coding RNAs, and metabolites, collectively known as the messenger ribonucleoprotein particle (mRNP). Its formation comprises the production of a mRNA precursor by RNA polymerase II and its processing by capping, splicing, and polyadenylation. Maturation of mRNA in the nucleus is the pre-requisite for its subsequent transport to, and localization within, the cytoplasm, where translation occurs. During these processes, the mRNA attracts and ejects *trans*-acting factors that make up the mRNP and are crucial for the respective phase.

Although many individual mRNA processing steps can be recapitulated *in vitro*, they are coupled *in vivo* to increase their efficiency and fidelity. The transcription-export (TREX) complex fulfills such function in nuclear mRNA biogenesis.[1–6] Components of TREX are functionally linked to each mRNA processing step, and this is reflected by their physical association with protein modules such as the cap-binding complex, the exon junction complex, and 3′ end processing factors.[7–10] TREX consists of six core proteins termed THOC1, THOC2, THOC5–THOC7, and Tex1 (forming the THO complex [THOC]), as well as THO-associated factors including the DEAD-box RNA helicase UAP56 (DDX39B), the export factor ALY/REF, and CHTOP.[11–14] Its proper function is crucial for maintaining the cellular mRNA

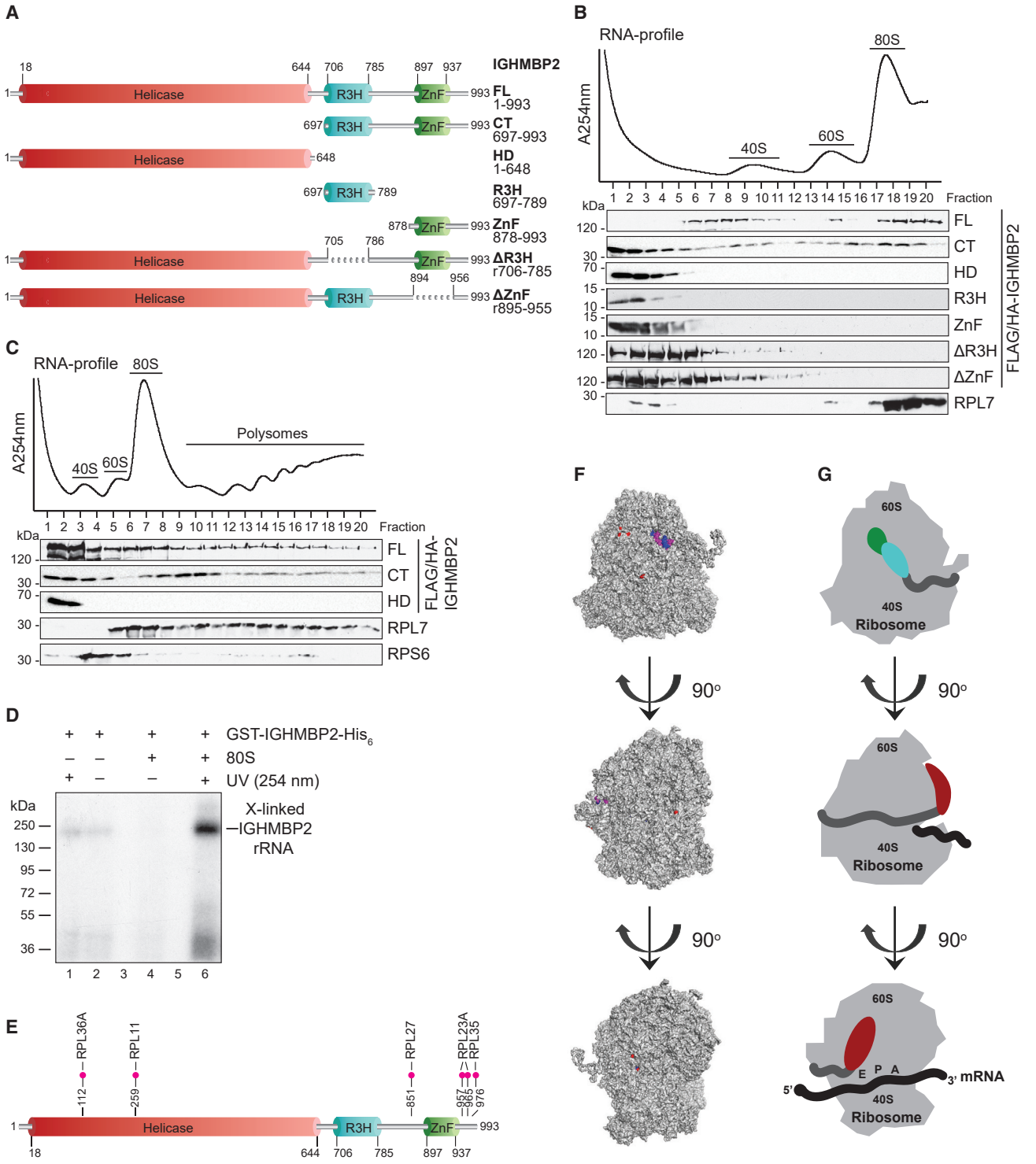

Figure 1. C terminus of IGHMBP2 is essential for 80S binding

(A) Schematic representation of IGHMBP2 domains and truncations/deletions.

(B) Density gradient centrifugation and western blot analysis of cell extracts after over-expression of different IGHMBP2 constructs to show interaction with 60S/80S fractions.

(C) Density gradient centrifugation and western blotting demonstrating that the C terminus weakly associates with polysomes.

(D) UV cross-linking and RNA radiolabeling using IGHMBP2/80S complexes (Figure S1B, lanes 10–12). Autoradiography of the SDS-PAGE shows a signal at the molecular weight of IGHMBP2 (lane 6), indicating a direct binding of IGHMBP2 to rRNA.

(legend continued on next page)

homeostasis, and its malfunction leads to various diseases including neurological disorders and cancer.[15–20]

Key players for the dynamic ATP-dependent remodeling of mRNPs during different phases of their cellular life are members of the RNA helicase enzyme family (reviewed in Fairman-Williams et al.,[21] Bourgeois et al.,[22] and Steimer and Klostermeier[23]). One helicase implicated in RNA metabolism is the immunoglobulin μ-binding protein 2 (IGHMBP2) belonging to UPF1-like helicase superfamily 1.[21,24] Mutations in the *IGHMBP2* gene resulting in the reduced formation of functional IGHMBP2 protein cause the autosomal recessive disorder spinal muscular atrophy with respiratory distress type 1 (SMARD1; also known as DSMA1). SMARD1 is characterized by distal skeletal muscle weakness and respiratory distress resulting from the degeneration of α-motor neurons in the spinal cord.[25–28] Early studies suggested a role for IGHMBP2 as an ATP-dependent DNA helicase involved in replication, transcription, and pre-mRNA splicing.[29–34] More recent studies, however, have demonstrated IGHMBP2 to be a 5′-3′ RNA helicase, involved in RNA metabolism, as a ribosome biogenesis factor as well as through its association with the ribosomes and tRNA.[35–37] SMARD1-causing mutations in *IGHMBP2* cluster in the helicase or ATPase domain of IGHMBP2 and generally impair either ATP binding and hydrolysis or RNA binding and unwinding, without affecting its ribosome association.[24,36] The cellular function of IGHMBP2 and therefore the molecular defects underlying SMARD1 have, however, remained enigmatic.

Here, we show that IGHMBP2 associates with polysomes and impacts the translation of mRNAs containing guanosine cytidine (GC)-rich, structured 5′ untranslated region (UTR). Strikingly, many of the deregulated mRNA targets encode for components of the THOC, linking IGHMBP2 to mRNA metabolism. Accordingly, ablation of IGHMBP2 causes specific perturbations in the cellular transcriptome and its encoded proteome. Of note, this effect is phenocopied by the forced reduction of the essential THOC subunits THOC1 and -2, showing that IGHMBP2 acts as an upstream regulator of THOC and consequently impacts cellular mRNA homeostasis. This regulation occurs in a cell-type-specific manner, as it is highly evident in reprogrammed induced astrocytes (iAs) but not in primary fibroblasts from patients with SMARD1 disease. Our results define IGHMBP2 as a crucial factor in cellular mRNA homeostasis acting through the THOC and suggest that its deregulation might be a biochemical defect contributing to the SMARD1 phenotype.

RESULTS

IGHMBP2 directly contacts the 60S ribosomal subunit through its C terminus

IGHMBP2 localizes to the cytoplasm, where it associates with ribosomes and polysomes.[35,36] To investigate how this association is established, we expressed in HEK Flp-In TREX cells FLAG/HA-IGHMBP2 full length, or truncations thereof, lacking either its N-terminal helicase domain, central R3H domain, or C-terminal zinc finger motif (Figure 1A). Cells were then lysed, and sedimentation of IGHMBP2 variants was analyzed by density gradient centrifugation (Figures 1B and 1C). As previously reported, IGHMBP2 co-sediments with 80S (Figure 1B) as well as polysomes (Figure 1C). Interestingly, the helicase domain failed to interact with ribosomes and polysomes and thus sedimented on top of the gradients. The C terminus (CT) containing the R3H and the ZnF domains known to be involved in RNA binding, in contrast, was necessary and sufficient for monosome co-sedimentation (Figure 1B). Both domains together are required for this interaction, as deletion of either one abolished their co-sedimentation with ribosomes (Figure 1B, ΔR3H, ΔZnF). Remarkably, despite its strong association with monosomes, the C terminus only weakly associates with polysomes (Figure 1C).

Next, we mapped the interaction site of IGHMBP2 on the ribosome. To detect potential RNA-binding sites, recombinant GST-IGHMBP2-His_6 was bound to isolated ribosomes *in vitro* (Figures S1A and S1B) and UV irradiated. After partial RNase digestion, the cross-linked rRNA fragments were identified by Illumina sequencing (Figure 1D). Two RNA fragments located at the 3′ and 5′ termini of 5.8S and 28S rRNAs, respectively, forming a duplex on the surface of the 60S large ribosomal subunit were identified as the main IGHMBP2 interaction sites (Figures 1F, 1G, and S1C; see Table S1 for additional minor cross-linking sites in 28S rRNA). Chemical cross-linking of the isolated native IGHMBP2-ribosome complex (Figure S1D) with Sulfo-DSS (BS3) and subsequent mass spectrometry revealed that the C terminus of IGHMBP2 contacts RPL23A, RPL27, and RPL35 (Figures 1E–1G; Table S2). These sites are near the identified 5.8S and 28S rRNA interaction sites and thus confirm the binding site of IGHMBP2 on the ribosome. Together, these data are consistent with a model by which IGHMBP2 is tethered to the rear surface of the ribosome, behind the P-site via a C-terminal binding module. The catalytic N-terminal domain appears not to be involved in ribosome binding but may rather be flexibly linked to the ribosome (Figures 1E–1G).

Complex alterations of the transcriptome upon IGHMBP2 depletion

The observed mode of interaction with the ribosome raised the possibility that IGHMBP2 targets mRNAs during translation. To test this notion, we generated IGHMBP2-deficient HeLa cells by small interfering RNA (siRNA)-mediated knockdown and analyzed polysome formation in comparison to wild-type cells. As determined by density gradient centrifugation, the polysome profiles of wild-type and IGHMBP2-deficient cells are largely identical (Figure S2A). IGHMBP2 is hence unlikely to act as a global regulator of the translation machinery. We next used a

(E) Illustration of cross-link sites on IGHMBP2 and the proteins they cross-link with on the ribosome identified by BS3 cross-linking and mass spectrometry analysis of native FLAG/HA-IGHMBP2-ribosome complex.
(F) Localization of 5.8S (magenta) and 28S (blue) rRNAs and RPLs (red) cross-links identified by Illumina sequencing and mass spectrometry, respectively, on human ribosome structure (PDB: 4UG0).
(G) Schematic representation of plausible mode of binding of IGHMBP2 to the ribosome based on RNA and protein cross-links.
See also Figure S1 and Tables S1 and S2.

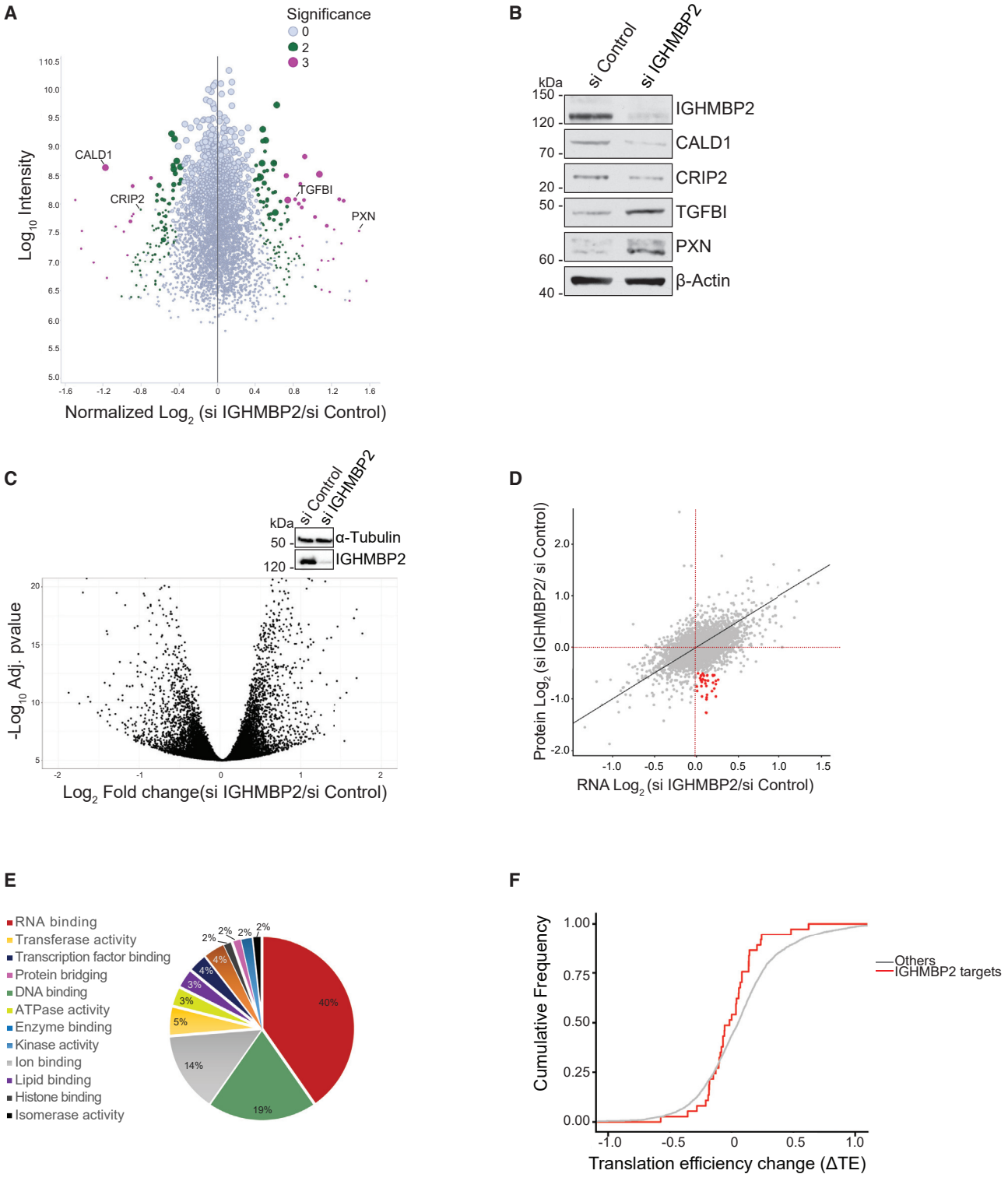

Figure 2. IGHMBP2 regulates translation of a subset of mRNAs

(A) Pulsed SILAC (pSILAC) analysis of control and IGHMBP2 knockdown cells from n = 2 independent biological replicates.

(B) Western blot analysis of pSILAC samples to confirm down-/upregulation of selected targets also indicated in (A).

(C) Volcano plot representation of RNA transcriptomics after IGHMBP2 knockdown from n = 3 independent biological replicates. Top: western blot confirmation of IGHMBP2 knockdown.

(legend continued on next page)

pulsed stable isotope labeling by amino acids in cell culture (pSILAC) approach to test whether IGHMBP2 specifically affects translation of a defined subset of cellular mRNAs. We differently labeled control and IGHMBP2 knockdown cells for 24 h using Lys-8/Arg-10 and Lys-4/Arg-6, respectively. Cell extracts were then analyzed by mass spectrometry and differentially translated proteins identified. Expression of most cellular proteins remained unchanged. Yet, interestingly, a specific set of proteins displayed a $\log_2$ fold change of over 0.75 (45 downregulated and 45 upregulated) upon IGHMBP2 knockdown, several of which have reported roles in neuromuscular development and cell morphology (Figures 2A and 2B; Table S3).

We next investigated whether the observed changes in protein levels upon IGHMBP2 knockdown are a consequence of translational regulation, mRNA abundance, or both. RNA sequencing (RNA-seq) analysis of control and IGHMBP2 knockdown cells showed that a similar number of transcripts displayed altered expression as compared to alterations in the proteome (Figure 2C). Importantly, correlation of RNA-seq and pSILAC data revealed that most of the observed alterations in protein levels upon IGHMBP2 depletion, both up- and downregulation, were a consequence of altered mRNA abundance (correlation coefficient $R = 0.55$, $p < 2.2 \times 10^{-16}$, bottom left and top right quadrants in Figure S2B). This is confirmed by RT-qPCR analysis of selected transcripts encoding the downregulated proteins shown in Figure 2B (Figure S2C). We also identified n = 63 genes with seemingly induced translation per mRNA ($\log_2$ fold change protein – $\log_2$ fold change RNA >0.5) and n = 144 genes with reduced translation per mRNA ($\log_2$ fold change protein – $\log_2$ fold change RNA < −0.5). Such a larger number of genes with reduced translation rates ($p = 3.8 \times 10^{-9}$, two-sided binomial test) suggests that knockdown of IGHMBP2 decreased the translation rates of a subset of genes. Particularly, a small group of 36 targets displayed significantly reduced protein levels ($\log_2$ fold change < −0.5) but was not downregulated at the mRNA level ($\log_2$ fold change >0, Figure 2D, shown in red, and 2E). We defined these 36 mRNAs as direct IGHMBP2 targets. Notably, many of them encode proteins linked to RNA metabolism. These include THOC1, THOC2, THOC5, THOC6, and CHTOP, all of which are crucial components of the TREX complex (see also Figure S2D for confirmation by western blotting). To corroborate the reduction in translation rates during IGHMBP2 deficiency inferred from comparing RNA-seq and pSILAC data, we performed ribosome profiling (Ribo-seq) in IGHMBP2 knockdown and control cells.[38] We calculated the translation efficiency (TE), i.e., the ratio of ribosome-protected fragments (RPFs) over the mRNA counts over the coding sequence of the transcript and then the change in TE (ΔTE) of the individual transcripts upon IGHMBP2 depletion.[39] Strikingly, the IGHMBP2 targets showed significantly reduced ΔTE values compared to all other genes ($p = 0.034$, two-sided Kolmogorov-Smirnov test, Figure 2F). We concluded that IGHMBP2 deficiency resulted in a significant reduction of translation rates for a small set of targets that included 5 components of the THOC.

IGHMBP2 regulates translation of THOC mRNAs through their 5′ UTRs

To investigate the mode of action of IGHMBP2 in translation regulation of its target mRNAs, we performed more in-depth analyses of the distribution of RPFs in our Ribo-seq data. We observed an altered RPF pattern in IGHMBP2-depleted cells on a global scale, with increased RPFs at the start codon followed by a drop immediately downstream spanning the next 25 codon triplets (Figure 3A). We defined a start codon stalling (SCS) score corresponding to the extent of the drop in RPFs in this region and subdivided all genes (n = 4,646) with detected translation into three categories according to the SCS score, namely strong (n = 1,528), weak (n = 2,476), and no SCS (n = 642). The 5′ UTR of genes with strong SCS were shorter, more GC-rich, and more highly structured than 5′ UTRs of genes with weak or no SCS (Figures S3A–S3C). Notably, the enrichment of RPFs over the rest of the coding sequence was unchanged during IGHMBP2 deficiency (Figure 3A). Surprisingly, among the identified 36 IGHMBP2 targets, only a third displayed strong SCS (see also Table S4) and the 5′ UTR signature. Importantly, the 5′ UTR signature that results in SCS upon IGHMBP2 depletion was also found in THOC1 and THOC2 transcripts (Figure S3D), and these transcripts also demonstrated SCS in Ribo-seq analysis. The expression of the peripheral components of the THOC including THOC5 and THOC6, however, appears to be regulated by a different mechanism that is dependent on the abundance of THOC1 and THOC2 (Figure S4A).

Next, we established a dual-luciferase assay system to confirm 5′ UTR-dependent translational regulation by IGHMBP2. We introduced the 5′ UTRs of THOC1 or THOC2 upstream of the firefly luciferase coding sequence and used Renilla luciferase for normalization. As controls, we tested highly structured 5′ UTRs like IGHMBP2-target UTRs arising from palindromic sequences or a 28-nucleotide-long poly-U unstructured 5′ UTR or without any 5′ UTR upstream of the firefly luciferase sequence (Figure S4B). We transfected control and IGHMBP2 knockdown cells with these different luciferase constructs, prepared cell extracts after 24 h, and tested these in dual-luciferase assay (Figure S4C). Introduction of THOC 5′ UTRs as well as the highly structured 5′ UTR upstream of firefly luciferase decreased its activity as compared to the control lacking any 5′ UTR or with an unstructured 5′ UTR in an IGHMBP2-dependent manner and thus confirms our findings (Figure 3B).

To investigate whether the proximal coding sequence of the mRNAs plays a role in IGHMBP2-dependent SCS and translation regulation, we introduced either the first 10 codons of THOC1 or THOC2 or a random 10 amino acid epitope-tag sequence (Myc-tag) between the 5′ UTR and the firefly luciferase coding sequence. In keeping with our Ribo-seq analysis, the presence

(D) Comparison of pSILAC and RNA sequencing datasets after IGHMBP2 knockdown, wherein red dots indicate proteins downregulated during translation after IGHMBP2 knockdown.
(E) Gene Ontology analysis of protein candidates downregulated during translation.
(F) Change in translation efficiency of direct targets of IGHMBP2 identified from pSILAC and transcriptomics as compared to all other transcripts.
See also Figure S2 and Tables S3 and S4.

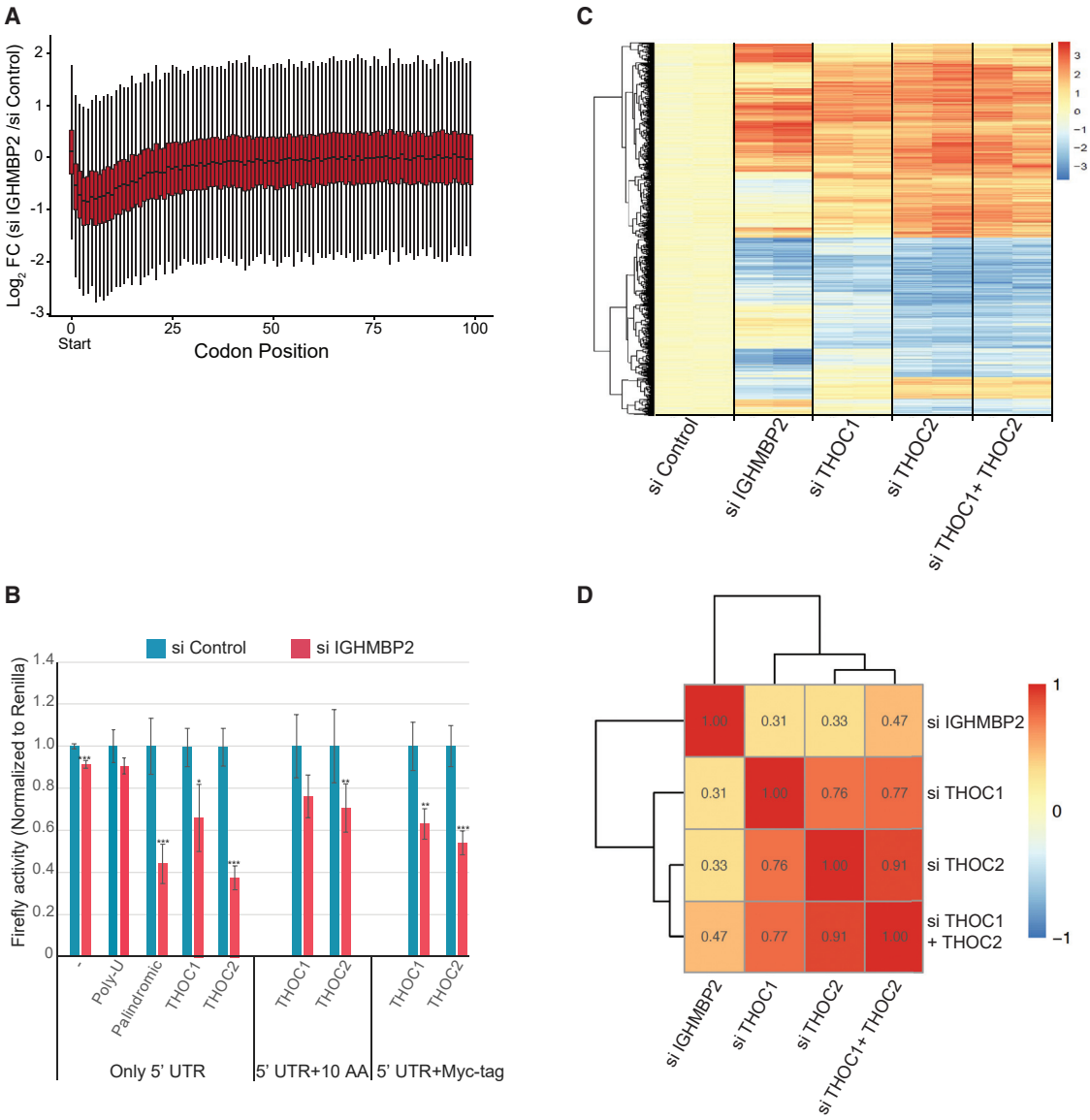

Figure 3. Translational targets of IGHMBP2 modulate RNA homeostasis

(A) Alterations in ribosome footprint profile on all transcripts during IGHMBP2 knockdown from n = 2 independent biological replicates.

(B) Dual-luciferase assay to mimic the effect of THOC 5′ UTRs on IGHMBP2-dependent translation from n = 3 independent biological replicates. Data are represented as mean ± SEM. *p < 0.1, **p < 0.05, and ***p < 0.01.

(C) Heatmap representation of comparison of cellular transcriptome after IGHMBP2 or THOC knockdown from n = 2 independent biological replicates.

(D) Representation of correlation coefficient of the different sets of knockdown conditions.

See also Figures S3 and S4 and Table S4.

of different coding sequences did not influence the downregulation of firefly luciferase expression observed in a 5′ UTR-dependent manner during IGHMBP2 knockdown (Figure 3B). Together, our data identify IGHMBP2 as a factor that specifically affects the translation of a very small and defined subset of mRNAs encoding proteins with roles in RNA metabolism.

THOC inactivation phenocopies IGHMBP2 deficiency

The THOC is part of the TREX complex and, as such, plays a crucial role in post-transcriptional mRNA biogenesis. The majority of the changes in cellular RNA homeostasis upon IGHMBP2 knockdown may hence be caused by the translational downregulation of the THO subunits. To test this model directly, we asked whether inactivation of THOC1 and/or THOC2 phenocopies the changes in mRNA metabolism during IGHMBP2 deficiency. Both THOC subunits were depleted from cells either individually or in combination (Figure S4A), and transcriptome profiles were generated by RNA-seq. Of note, while depletion of THOC2 resulted in the downregulation of other THOC components, knockdown of THOC1 did not affect the expression of

THOC2 but downregulated the expression of THOC5 and THOC6 (Figure S4A). Importantly, the expression of IGHMBP2 was unaffected during THOC depletion, and hence the resulting changes in the transcriptome are IGHMBP2 independent. These datasets were then compared with corresponding datasets obtained from control and IGHMBP2-depleted cells (Figures 3C and 3D).

The knockdown of either THOC1 or THOC2 affected the expression level of a very similar set of transcripts (correlation coefficient R = 0.76) and so did their combined knockdown (Figures 3C and 3D), confirming that both factors act in the same pathway. Interestingly, THOC2-depleted cells showed a better correlation to the dual knockdown (correlation coefficient R = 0.91, Figures 3C and 3D) than THOC1 depletion alone (correlation coefficient R = 0.77, Figures 3C and 3D), as THOC2 knockdown also resulted in the indirect downregulation of THOC1 due to yet-unknown mechanisms (Figure S4A). Strikingly, the transcriptome profiles of THOC1- and THOC2-depleted cells were also highly similar to IGHMBP2-depleted cells, with a correlation coefficient R = 0.47 (Figure 3D). Several of the strongly downregulated mRNAs common to the three conditions play crucial roles in cell proliferation, regulation of apoptosis, aging, and lipid metabolism.

The observed changes in the cellular RNA pool might be the result of alterations in transcription, stability, or a combination thereof. To investigate these scenarios, we analyzed candidate mRNAs downregulated in both IGHMBP2 and THOC deficiencies using RT-qPCR and exosome inhibition using 5-fluorouracil. Although the expression of some of these mRNAs recovered upon exosome inhibition, implying RNA degradation as the underlying cause for the observed effects, others were unaffected by exosome inhibition (Figure S4D). These data suggest a combination of transcriptional and post-transcriptional RNA regulation as the underlying cause of altered RNA homeostasis during both IGHMBP2 and THOC deficiencies.

Induced astrocytes from patients with SMARD1 disease demonstrate THOC regulation

Our data have uncovered an unexpected link between IGHMBP2 and the translational regulation of key factors of THOC. We hence reasoned that similar events may also occur in cells derived from patients with SMARD1 disease, which display drastically reduced IGHMBP2 levels. Primary fibroblasts were collected from patients, and an *in vitro* cell reprogramming protocol was used to convert them into functional induced astrocytes (iAs).[40] We focused on astrocytes since SMARD1 is a neurodegenerative disease and this method has a been used in multiple neurological disorders successfully to study disease mechanisms and test novel therapeutics.[41,42] The analysis of induced astrocytes derived from a patient with SMARD1 disease (mutations in *IGHMBP2*, c.1432G>A, p.Val478Met and c.1082 T>C, p.Leu361-Pro) showed a drastic downregulation of THOC1 and THOC2, which was not observed in cells of healthy individuals (Figures 4A and 4B). Interestingly, another patient with nearly identical phenotypic manifestation of neurodegenerative disease, initially assessed as likely suffering from SMARD1, but later genotypically characterized otherwise (mutation in *CFP* (Complement Factor Properdin), homozygous, c.1010G>A, p.Cys337Tyr) also showed a downregulation in the expression of THOC1 although to a lesser extent while THOC2 and IGHMBP2 levels remained unchanged (Figures 4A and 4B). It is therefore highly plausible that the deregulation of THOC components affect downstream cellular gene expression in similar ways in both the neurodegenerative diseases. Furthermore we tested the expression of THOC components in another patient with SMARD1 disease (mutations in *IGHMBP2*, c.1488C>A, p.Cys496* and c.1478C>T, p.Thr493Ile) and found THOC1 and THOC2 to be downregulated (Figures S5A and S5B). We then sought to rescue the expression of THOC in these SMARD1 iAs using adeno-associated virus expressing IGHMBP2 (AAV9.IGHMBP2, ClinicalTrials.gov: NCT05152823) transduction, which was previously reported to restore neurite length in SMARD1-induced neurons.[43] Surprisingly, although we observed a clear recovery of THOC1 and THOC2 expression in SMARD1 iAs 4342, this was not observed in the second SMARD1 iAs 208 (Figures S5A and S5B). One likely scenario is that different cells (as is likely the case also with patients) need to be treated with AAV9.IGHMBP2 for varied periods of time, depending on disease severity, to restore molecular function of IGHMBP2 and, thereby, THOC expression.

Although IGHMBP2 is a ubiquitously expressed protein, patients with SMARD1 disease display a highly tissue specific phenotype where neuronal tissue is primarily affected. It was hence interesting to ask whether the observed THOC regulation by IGHMBP2 is a general, rather than cell-type-specific, phenomenon. We therefore performed siRNA-mediated knockdown of IGHMBP2 in different cell types and tested THOC expression by western blotting (Figure S5C). In contrast to our expectation, downregulation of THOC was evident only in a few cell types, indicating a cell-specific regulatory event (Figure S5C). Interestingly, among the different cell lines tested, we observed this regulation in primary cells and those of neuronal origin. It is therefore plausible that motor neuron defects observed in patients with SMARD1 disease arise from strong downregulation of THOC in neuronal cells.

DISCUSSION

The association of IGHMBP2 with ribosomes and tRNAs shown in previous studies suggested a role for this helicase in the context of translation.[35,36] Results from this study confirm these earlier findings and reveal an unexpected molecular function for IGHMBP2.

Here, we showed that IGHMBP2 strongly influences the cellular transcriptome. Interestingly, however, this effect is secondary and can be attributed to the direct regulation of only a very small group of mRNAs at the translation level. Many of these direct targets of IGHMBP2 encode proteins involved in RNA metabolism, whereby it is particularly obvious that five key components of the THOC are among the regulated targets. Together with other factors, the THOC forms the TREX complex, which is largely responsible for the coupling of mRNA transcription and export and thus for the homeostasis of the cellular mRNA pool. Indeed, inhibition of TREX function by siRNA-mediated depletion of THOC1 and THOC2 leads to a very similar deregulation of mRNA homeostasis as observed by the reduction of IGHMBP2. Our data therefore identify IGHMBP2 as a regulator

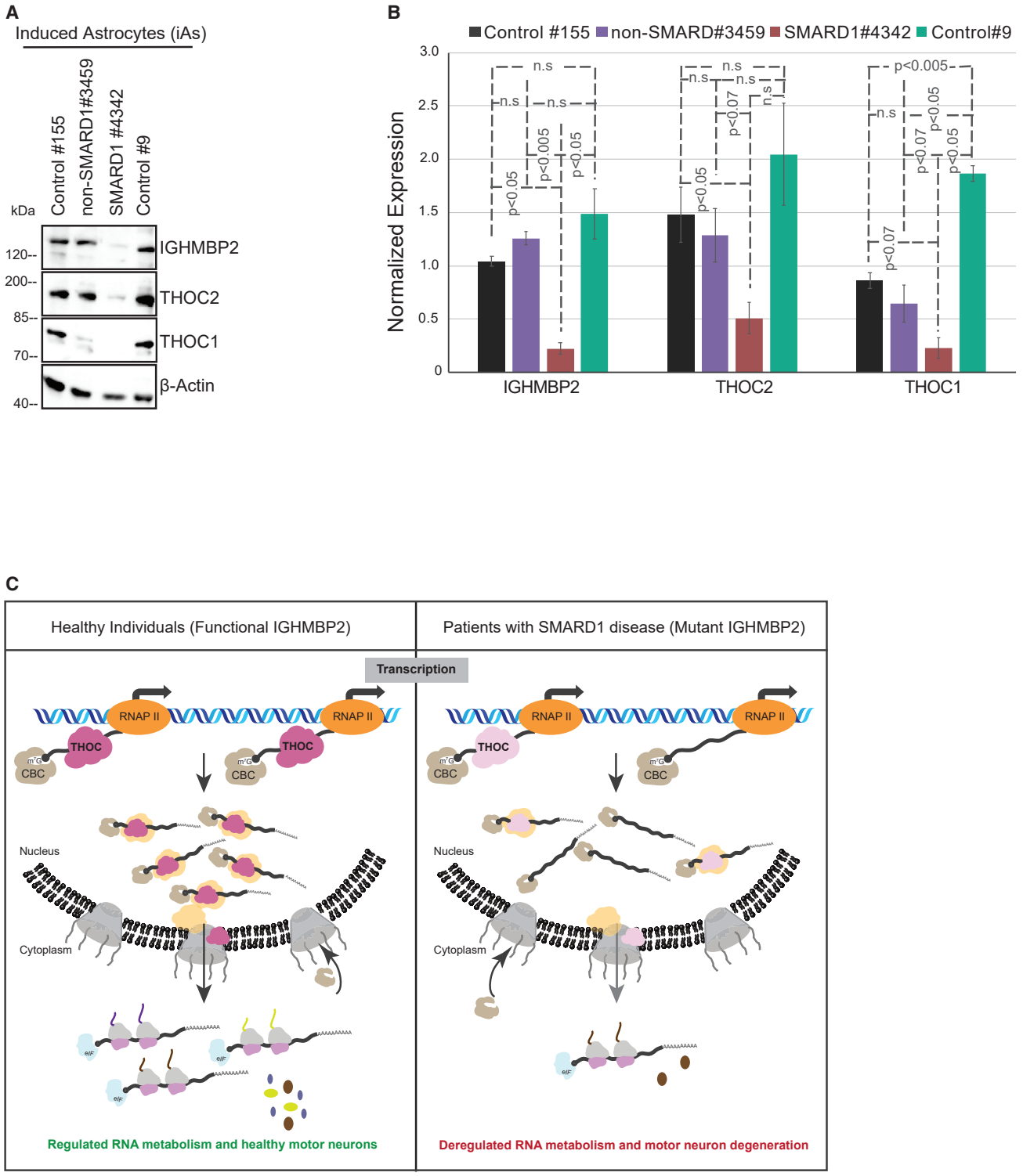

Figure 4. The THOC is deregulated in astrocytes derived from patients with SMARD1 disease

(A) Western blot analysis of THOC in induced astrocytes from healthy individuals (control) and patients with SMARD1 or another neuronal disease.

(B) Quantification of western blot shown in (A) from n = 3 independent biological replicates. Data are represented as mean ± SEM.

(C) Proposed model demonstrating how absence of functional IGHMBP2 results in THOC deregulation and thereby cellular RNA and protein homeostasis in patients with SMARD1 disease.

See also Figure S5.

of mRNA metabolism acting upstream of the TREX complex. The deregulation of mRNA metabolism is, in this scenario, a consequence of both transcriptional downregulation of downstream targets as well as the failure of TREX to export newly transcribed mRNAs to the cytoplasm (Figure 4C).

The way in which IGHMBP2 associates with the ribosome gives a first indication of how this helicase might affect translation of target mRNAs. Our *in vitro* interaction studies and UV cross-linking revealed that the putative RNA-binding R3H and ZnF domains in the C terminus of IGHMBP2 are necessary and sufficient to mediate ribosome association. In contrast, the N-terminal catalytic helicase domain appears to be flexibly connected to this C-terminal "anchor." Our inability to localize IGHMBP2 to the ribosome via cryo-EM studies confirms this flexible and bi-modular binding. This binding mode would potentially allow the helicase domain to be brought into proximity of the ribosome-bound mRNAs so that regulation through IGHMBP2 can be enabled. Clearly, a high-resolution structural snapshot of IGHMBP2 at the ribosome would help to validate this attractive model.

Over the years, several lines of evidence have evolved in favor of eukaryotic RNA regulons or post-transcriptional operons, originally proposed as "informosomes" by Spirin and co-workers. According to their model, sequence-specific RBPs can regulate functionally related mRNAs as subpopulations to aid in the coordinated expression of those proteins involved in the same cellular pathway.[44–47] Our results indicate that THOC-encoding mRNAs are co-regulated during translation by IGHMBP2, where the length, GC content, and secondary structure of the 5′ UTR of messages function as the defining features of the RNA regulon for THOC expression.

IGHMBP2-related helicases may regulate translation either in a general or target-specific manner. eIF4A is a well-known example for the former, as it acts as part of the eIF4F complex in 40S scanning in a target-independent manner.[48] Target-specific RNA helicases, in contrast, regulate defined mRNAs by various mechanisms. Well-known examples are DHX9, which binds to and resolves the post-transcriptional control element in the 5′ UTR of target mRNAs and Vasa, which has been shown to aid translation initiation by binding to U-rich elements in 3′ UTR to enable 60S subunit joining with the 40S.[49,50]

According to our results, IGHMBP2 is a target-specific RNA helicase, but how it identifies and regulates the mRNAs is still an open question. Our data suggest that IGHMBP2 is not a stoichiometric component of ribosomes. However, majority of cellular IGHMBP2 is associated with the translation machinery at steady state. Preliminary experiments performed by arresting the 48S pre-initiation complex using the non-hydrolyzable GTP analog GMPPNP showed that IGHMBP2 was not part of the pre-initiation complex and was recruited along with the 60S to the translation system (Figure S5D). IGHMBP2 may hence become selectively recruited along with 60S to the small ribosomal subunit at the start codon of bound mRNAs and is poised to begin translation. Our ribosomal profiling data indicate that stalling occurs at the start codon of target mRNAs during IGHMBP2 deficiency, which would be consistent with this scenario. We therefore hypothesize that IGHMBP2 might be involved in ribosome subunit joining at the start codon, where certain 5′ UTR structures might result in steric interference for 40S-60S interaction (Figure S5E).

IGHMBP2 has long been in the focus of biomedical research because of its link to the neuromuscular disease SMARD1. Indeed, our previous studies have shown that loss of its helicase function is alone sufficient to cause the disease phenotype.[26] SMARD1 is a disease that shows a "tissue-specificity paradox," i.e., only very few cell types (including motor neurons) are primarily affected in patients even though IGHMBP2 is a ubiquitously expressed protein. Interestingly, our studies have shown that deregulation of the THOC, and thereby mRNA metabolism as a consequence of IGHMBP2 deficiency, is only observed in specific cell types, including those of neuronal origin. It remains to be seen to what extent the disruption in mRNA metabolism we have described contributes to the etiology of the disease, and such studies are currently in progress.

Limitations of the study

We used cell-culture-based models and targeted knockdown of IGHMBP2 to understand the molecular function of this protein in the onset of SMARD1. Our results suggest a cell-type-specific regulation of THOC expression by IGHMBP2. Patient-derived induced astrocytes demonstrated similar regulation of THOC components. If this also applies to motor neurons, the cell type primarily affected in SMARD1 remains to be seen. Furthermore, whether the observed transcriptome alterations can be rescued by exogenous expression of the THOC, and if this can be used as an alternate therapeutic approach in SMARD1, needs further investigation.

STAR★METHODS

Detailed methods are provided in the online version of this paper and include the following:

- KEY RESOURCES TABLE
- RESOURCE AVAILABILITY
  - Lead contact
  - Materials availability
  - Data and code availability
- EXPERIMENTAL MODEL AND STUDY PARTICIPANT DETAILS
  - Cell lines
  - Primary cell cultures
  - Bacterial cells
- METHOD DETAILS
  - Cell culture and RNAi-mediated knockdown
  - Mono/polysome density gradient centrifugation
  - Purification of recombinant IGHMBP2
  - Purification of 80S ribosomes
  - *In vitro* IGHMBP2-ribosome CLIP
  - Pulsed-SILAC labeling and mass spectrometry
  - Purification of FLAG/HA-IGHMBP2-ribosomes
  - IGHMBP2-80S BS3 cross-linking and CXMS
  - CXMS data analysis
  - RNA extraction and RT-qPCR
  - RNA-seq, Ribo-seq and data processing
  - Dual-luciferase vectors and luciferase assay
  - Primary fibroblasts and induced astrocytes
- QUANTIFICATION AND STATISTICAL ANALYSIS

SUPPLEMENTAL INFORMATION

Supplemental information can be found online at https://doi.org/10.1016/j.celrep.2024.113802.

ACKNOWLEDGMENTS

We thank Prof. Niels Gehring for the kind gift of antibodies, Dr. Kevin Flanigan from Nationwide Children's Hospital for collecting skin biopsies from patients with SMARD1 disease and healthy individuals, Dr. Andreas Linden for help with BS3 mass spectrometry analysis, Dr. Clemens Grimm for help with structural illustration of protein and RNA cross-linking data, Dr. Cornelius Schneider for critical reading of the manuscript, and Dr. Georg Stoll and Dr. Ashwin Chari for help with ribosome sample preparation. RNA-seq was performed at the Core Unit System Medicine of the University of Würzburg by Dr. Panagiota Arampatzi. We thank Ms. Elisabeth Kunkel, Ms. Stephanie Lamar, Ms. Monika Raabe, and Ms. Pradhipa Ramanathan for technical help with experiments. This work was supported by DFG (Fi 573/15-2 to U.F. and JA 1823/5-1 to S.J.), NIH P50 (P50AR070604 to K.C.M.), SMASHSMARD USA and SMASHSMARD Germany to K.C.M., and SMASHSMARD Germany to S.J.

AUTHOR CONTRIBUTIONS

A.B.P., A.H., and U.F. conceived and designed the experiments. A.B.P. and A.H. carried out all the experiments. U.-P.G. processed samples for Ribo-seq, A.S. carried out pSILAC mass spectrometry analysis, H.H. purified the complex for BS3 cross-linking, O.D. and H.U. performed mass spectrometry analysis of BS3 cross-linked samples, J.A.S.-D. and K.C.M. established iAs cell culture from patient fibroblasts, S.J. and E.Y. processed samples for siIGHMBP2 RNA-seq, and F.E. did bioinformatic analysis of all data. A.B.P. and U.F. analyzed the data and wrote the manuscript. The manuscript was seen and approved by all authors.

DECLARATION OF INTERESTS

The authors declare no competing interests.

Received: August 3, 2023
Revised: December 21, 2023
Accepted: January 31, 2024
Published: February 17, 2024

REFERENCES

1. Guria, A., Tran, D.D.H., Ramachandran, S., Koch, A., El Bounkari, O., Dutta, P., Hauser, H., and Tamura, T. (2011). Identification of mRNAs that are spliced but not exported to the cytoplasm in the absence of THOC5 in mouse embryo fibroblasts. RNA *17*, 1048–1056. https://doi.org/10.1261/rna.2607011.
2. Saran, S., Tran, D.D.H., Klebba-Färber, S., Moran-Losada, P., Wiehlmann, L., Koch, A., Chopra, H., Pabst, O., Hoffmann, A., Klopfleisch, R., and Tamura, T. (2013). THOC5, a member of the mRNA export complex, contributes to processing of a subset of wingless/integrated (Wnt) target mRNAs and integrity of the gut epithelial barrier. BMC Cell Biol. *14*, 51. https://doi.org/10.1186/1471-2121-14-51.
3. Tran, D.D.H., Saran, S., Williamson, A.J.K., Pierce, A., Dittrich-Breiholz, O., Wiehlmann, L., Koch, A., Whetton, A.D., and Tamura, T. (2014). THOC5 controls 3'end-processing of immediate early genes via interaction with polyadenylation specific factor 100 (CPSF100). Nucleic Acids Res. *42*, 12249–12260. https://doi.org/10.1093/nar/gku911.
4. Tran, D.D.H., Saran, S., Dittrich-Breiholz, O., Williamson, A.J.K., Klebba-Färber, S., Koch, A., Kracht, M., Whetton, A.D., and Tamura, T. (2013). Transcriptional regulation of immediate-early gene response by THOC5, a member of mRNA export complex, contributes to the M-CSF-induced macrophage differentiation. Cell Death Dis. *4*, e879. https://doi.org/10.1038/cddis.2013.409.
5. Wang, L., Miao, Y.L., Zheng, X., Lackford, B., Zhou, B., Han, L., Yao, C., Ward, J.M., Burkholder, A., Lipchina, I., et al. (2013). The THO complex regulates pluripotency gene mRNA export and controls embryonic stem cell self-renewal and somatic cell reprogramming. Cell Stem Cell *13*, 676–690. https://doi.org/10.1016/j.stem.2013.10.008.
6. Maeder, C.I., Kim, J.I., Liang, X., Kaganovsky, K., Shen, A., Li, Q., Li, Z., Wang, S., Xu, X.Z.S., Li, J.B., et al. (2018). The THO Complex Coordinates Transcripts for Synapse Development and Dopamine Neuron Survival. Cell *174*, 1436–1449.e20. https://doi.org/10.1016/j.cell.2018.07.046.
7. Pacheco-Fiallos, B., Vorländer, M.K., Riabov-Bassat, D., Fin, L., O'Reilly, F.J., Ayala, F.I., Schellhaas, U., Rappsilber, J., and Plaschka, C. (2023). mRNA recognition and packaging by the human transcription-export complex. Nature *616*, 828–835. https://doi.org/10.1038/s41586-023-05904-0.
8. Pühringer, T., Hohmann, U., Fin, L., Pacheco-Fiallos, B., Schellhaas, U., Brennecke, J., and Plaschka, C. (2020). Structure of the human core transcription-export complex reveals a hub for multivalent interactions. Elife *9*, e61503. https://doi.org/10.7554/eLife.61503.
9. Viphakone, N., Sudbery, I., Griffith, L., Heath, C.G., Sims, D., and Wilson, S.A. (2019). Co-transcriptional Loading of RNA Export Factors Shapes the Human Transcriptome. Mol. Cell *75*, 310–323.e8. https://doi.org/10.1016/j.molcel.2019.04.034.
10. Hautbergue, G.M., Hung, M.L., Golovanov, A.P., Lian, L.Y., and Wilson, S.A. (2008). Mutually exclusive interactions drive handover of mRNA from export adaptors to TAP. Proc. Natl. Acad. Sci. USA *105*, 5154–5159. https://doi.org/10.1073/pnas.0709167105.
11. Heath, C.G., Viphakone, N., and Wilson, S.A. (2016). The role of TREX in gene expression and disease. Biochem. J. *473*, 2911–2935. https://doi.org/10.1042/BCJ20160010.
12. Dufu, K., Livingstone, M.J., Seebacher, J., Gygi, S.P., Wilson, S.A., and Reed, R. (2010). ATP is required for interactions between UAP56 and two conserved mRNA export proteins, Aly and CIP29, to assemble the TREX complex. Genes Dev. *24*, 2043–2053. https://doi.org/10.1101/gad.1898610.
13. Strässer, K., Masuda, S., Mason, P., Pfannstiel, J., Oppizzi, M., Rodriguez-Navarro, S., Rondón, A.G., Aguilera, A., Struhl, K., Reed, R., and Hurt, E. (2002). TREX is a conserved complex coupling transcription with messenger RNA export. Nature *417*, 304–308. https://doi.org/10.1038/nature746.
14. Gromadzka, A.M., Steckelberg, A.L., Singh, K.K., Hofmann, K., and Gehring, N.H. (2016). A short conserved motif in ALYREF directs cap- and EJC-dependent assembly of export complexes on spliced mRNAs. Nucleic Acids Res. *44*, 2348–2361. https://doi.org/10.1093/nar/gkw009.
15. Beaulieu, C.L., Huang, L., Innes, A.M., Akimenko, M.A., Puffenberger, E.G., Schwartz, C., Jerry, P., Ober, C., Hegele, R.A., McLeod, D.R., et al. (2013). Intellectual disability associated with a homozygous missense mutation in THOC6. Orphanet J. Rare Dis. *8*, 62. https://doi.org/10.1186/1750-1172-8-62.
16. Boycott, K.M., Beaulieu, C., Puffenberger, E.G., McLeod, D.R., Parboosingh, J.S., and Innes, A.M. (2010). A novel autosomal recessive malformation syndrome associated with developmental delay and distinctive facies maps to 16ptel in the Hutterite population. Am. J. Med. Genet. *152A*, 1349–1356. https://doi.org/10.1002/ajmg.a.33379.
17. Kumar, R., Corbett, M.A., van Bon, B.W.M., Woenig, J.A., Weir, L., Douglas, E., Friend, K.L., Gardner, A., Shaw, M., Jolly, L.A., et al. (2015). THOC2 Mutations Implicate mRNA-Export Pathway in X-Linked Intellectual Disability. Am. J. Hum. Genet. *97*, 302–310. https://doi.org/10.1016/j.ajhg.2015.05.021.
18. Kumar, R., Gardner, A., Homan, C.C., Douglas, E., Mefford, H., Wieczorek, D., Lüdecke, H.J., Stark, Z., Sadedin, S., et al.; Broad CMG (2018). Severe neurocognitive and growth disorders due to variation in THOC2, an essential component of nuclear mRNA export machinery. Hum. Mutat. *39*, 1126–1138. https://doi.org/10.1002/humu.23557.

19. Saran, S., Tran, D.D.H., Ewald, F., Koch, A., Hoffmann, A., Koch, M., Nashan, B., and Tamura, T. (2016). Depletion of three combined THOC5 mRNA export protein target genes synergistically induces human hepatocellular carcinoma cell death. Oncogene *35*, 3872–3879. https://doi.org/10.1038/onc.2015.433.

20. Zhou, X., Liu, X., Zhang, G., Zhang, Q., Chen, H., Wang, Y., Fang, F., and Sun, J. (2019). Knockdown THOC2 suppresses the proliferation and invasion of melanoma. Bioengineered *10*, 635–645. https://doi.org/10.1080/21655979.2019.1685727.

21. Fairman-Williams, M.E., Guenther, U.P., and Jankowsky, E. (2010). SF1 and SF2 helicases: family matters. Curr. Opin. Struct. Biol. *20*, 313–324. https://doi.org/10.1016/j.sbi.2010.03.011.

22. Bourgeois, C.F., Mortreux, F., and Auboeuf, D. (2016). The multiple functions of RNA helicases as drivers and regulators of gene expression. Nat. Rev. Mol. Cell Biol. *17*, 426–438. https://doi.org/10.1038/nrm.2016.50.

23. Steimer, L., and Klostermeier, D. (2012). RNA helicases in infection and disease. RNA Biol. *9*, 751–771. https://doi.org/10.4161/rna.20090.

24. Lim, S.C., Bowler, M.W., Lai, T.F., and Song, H. (2012). The Ighmbp2 helicase structure reveals the molecular basis for disease-causing mutations in DMSA1. Nucleic Acids Res. *40*, 11009–11022. https://doi.org/10.1093/nar/gks792.

25. Grohmann, K., Varon, R., Stolz, P., Schuelke, M., Janetzki, C., Bertini, E., Bushby, K., Muntoni, F., Ouvrier, R., Van Maldergem, L., et al. (2003). Infantile spinal muscular atrophy with respiratory distress type 1 (SMARD1). Ann. Neurol. *54*, 719–724. https://doi.org/10.1002/ana.10755.

26. Guenther, U.P., Varon, R., Schlicke, M., Dutrannoy, V., Volk, A., Hübner, C., von Au, K., and Schuelke, M. (2007). Clinical and mutational profile in spinal muscular atrophy with respiratory distress (SMARD): defining novel phenotypes through hierarchical cluster analysis. Hum. Mutat. *28*, 808–815. https://doi.org/10.1002/humu.20525.

27. Maystadt, I., Zarhrate, M., Landrieu, P., Boespflug-Tanguy, O., Sukno, S., Collignon, P., Melki, J., Verellen-Dumoulin, C., Munnich, A., and Viollet, L. (2004). Allelic heterogeneity of SMARD1 at the IGHMBP2 locus. Hum. Mutat. *23*, 525–526. https://doi.org/10.1002/humu.9241.

28. Wilmshurst, J.M., Bye, A., Rittey, C., Adams, C., Hahn, A.F., Ramsay, D., Pamphlett, R., Pollard, J.D., and Ouvrier, R. (2001). Severe infantile axonal neuropathy with respiratory failure. Muscle Nerve *24*, 760–768. https://doi.org/10.1002/mus.1067.

29. Biswas, E.E., Nagele, R.G., and Biswas, S. (2001). A novel human hexameric DNA helicase: expression, purification and characterization. Nucleic Acids Res. *29*, 1733–1740. https://doi.org/10.1093/nar/29.8.1733.

30. Fukita, Y., Mizuta, T.R., Shirozu, M., Ozawa, K., Shimizu, A., and Honjo, T. (1993). The human S mu bp-2, a DNA-binding protein specific to the single-stranded guanine-rich sequence related to the immunoglobulin mu chain switch region. J. Biol. Chem. *268*, 17463–17470.

31. Mizuta, T.R., Fukita, Y., Miyoshi, T., Shimizu, A., and Honjo, T. (1993). Isolation of cDNA encoding a binding protein specific to 5'-phosphorylated single-stranded DNA with G-rich sequences. Nucleic Acids Res. *21*, 1761–1766. https://doi.org/10.1093/nar/21.8.1761.

32. Molnar, G.M., Crozat, A., Kraeft, S.K., Dou, Q.P., Chen, L.B., and Pardee, A.B. (1997). Association of the mammalian helicase MAH with the pre-mRNA splicing complex. Proc. Natl. Acad. Sci. USA *94*, 7831–7836. https://doi.org/10.1073/pnas.94.15.7831.

33. Shieh, S.Y., Stellrecht, C.M., and Tsai, M.J. (1995). Molecular characterization of the rat insulin enhancer-binding complex 3b2. Cloning of a binding factor with putative helicase motifs. J. Biol. Chem. *270*, 21503–21508. https://doi.org/10.1074/jbc.270.37.21503.

34. Zhang, Q., Wang, Y.C., and Montalvo, E.A. (1999). Smubp-2 represses the Epstein-Barr virus lytic switch promoter. Virology *255*, 160–170. https://doi.org/10.1006/viro.1998.9588.

35. de Planell-Saguer, M., Schroeder, D.G., Rodicio, M.C., Cox, G.A., and Mourelatos, Z. (2009). Biochemical and genetic evidence for a role of IGHMBP2 in the translational machinery. Hum. Mol. Genet. *18*, 2115–2126. https://doi.org/10.1093/hmg/ddp134.

36. Guenther, U.P., Handoko, L., Laggerbauer, B., Jablonka, S., Chari, A., Alzheimer, M., Ohmer, J., Plöttner, O., Gehring, N., Sickmann, A., et al. (2009). IGHMBP2 is a ribosome-associated helicase inactive in the neuromuscular disorder distal SMA type 1 (DSMA1). Hum. Mol. Genet. *18*, 1288–1300. https://doi.org/10.1093/hmg/ddp028.

37. Vadla, G.P., Ricardez Hernandez, S.M., Mao, J., Garro-Kacher, M.O., Lorson, Z.C., Rice, R.P., Hansen, S.A., Lorson, C.L., Singh, K., and Lorson, M.A. (2023). ABT1 modifies SMARD1 pathology via interactions with IGHMBP2 and stimulation of ATPase and helicase activity. JCI Insight *8*, e164608. https://doi.org/10.1172/jci.insight.164608.

38. Ingolia, N.T., Brar, G.A., Rouskin, S., McGeachy, A.M., and Weissman, J.S. (2012). The ribosome profiling strategy for monitoring translation in vivo by deep sequencing of ribosome-protected mRNA fragments. Nat. Protoc. *7*, 1534–1550. https://doi.org/10.1038/nprot.2012.086.

39. Chothani, S., Adami, E., Ouyang, J.F., Viswanathan, S., Hubner, N., Cook, S.A., Schafer, S., and Rackham, O.J.L. (2019). deltaTE: Detection of Translationally Regulated Genes by Integrative Analysis of Ribo-seq and RNA-seq Data. Curr. Protoc. Mol. Biol. *129*, e108. https://doi.org/10.1002/cpmb.108.

40. Dennys, C.N., Sierra-Delgado, J.A., Ray, S.S., Hartlaub, A.M., Roussel, F.S., Rodriguez, Y., and Meyer, K. (2021). In vitro Modeling for Neurological Diseases using Direct Conversion from Fibroblasts to Neuronal Progenitor Cells and Differentiation into Astrocytes. J. Vis. Exp. https://doi.org/10.3791/62016.

41. Acioglu, C., Li, L., and Elkabes, S. (2021). Contribution of astrocytes to neuropathology of neurodegenerative diseases. Brain Res. *1758*, 147291. https://doi.org/10.1016/j.brainres.2021.147291.

42. de Rus Jacquet, A., Denis, H.L., Cicchetti, F., and Alpaugh, M. (2021). Current and future applications of induced pluripotent stem cell-based models to study pathological proteins in neurodegenerative disorders. Mol. Psychiatr. *26*, 2685–2706. https://doi.org/10.1038/s41380-020-00999-7.

43. Sierra-Delgado, J.A., Sinha-Ray, S., Kaleem, A., Ganjibakhsh, M., Parvate, M., Powers, S., Zhang, X., Likhite, S., and Meyer, K. (2023). In Vitro Modeling as a Tool for Testing Therapeutics for Spinal Muscular Atrophy and IGHMBP2-Related Disorders. Biology *12*. https://doi.org/10.3390/biology12060867.

44. Culjkovic-Kraljacic, B., and Borden, K.L.B. (2018). The Impact of Post-transcriptional Control: Better Living Through RNA Regulons. Front. Genet. *9*, 512. https://doi.org/10.3389/fgene.2018.00512.

45. Keene, J.D. (2007). RNA regulons: coordination of post-transcriptional events. Nat. Rev. Genet. *8*, 533–543. https://doi.org/10.1038/nrg2111.

46. Keene, J.D., and Tenenbaum, S.A. (2002). Eukaryotic mRNPs may represent posttranscriptional operons. Mol. Cell *9*, 1161–1167. https://doi.org/10.1016/s1097-2765(02)00559-2.

47. Spirin, A.S. (1969). The second Sir Hans Krebs Lecture. Informosomes. Eur. J. Biochem. *10*, 20–35. https://doi.org/10.1111/j.1432-1033.1969.tb00651.x.

48. Svitkin, Y.V., Pause, A., Haghighat, A., Pyronnet, S., Witherell, G., Belsham, G.J., and Sonenberg, N. (2001). The requirement for eukaryotic initiation factor 4A (eIF4A) in translation is in direct proportion to the degree of mRNA 5' secondary structure. RNA *7*, 382–394. https://doi.org/10.1017/s135583820100108x.

49. Hartman, T.R., Qian, S., Bolinger, C., Fernandez, S., Schoenberg, D.R., and Boris-Lawrie, K. (2006). RNA helicase A is necessary for translation of selected messenger RNAs. Nat. Struct. Mol. Biol. *13*, 509–516. https://doi.org/10.1038/nsmb1092.

50. Johnstone, O., and Lasko, P. (2004). Interaction with eIF5B is essential for Vasa function during development. Development *131*, 4167–4178. https://doi.org/10.1242/dev.01286.

51. Surrey, V., Zöller, C., Lork, A.A., Moradi, M., Balk, S., Dombert, B., Saal-Bauernschubert, L., Briese, M., Appenzeller, S., Fischer, U., and Jablonka, S. (2018). Impaired Local Translation of beta-actin mRNA in Ighmbp2-Deficient Motoneurons: Implications for Spinal Muscular Atrophy with respiratory Distress (SMARD1). Neuroscience *386*, 24–40. https://doi.org/10.1016/j.neuroscience.2018.06.019.

52. Perez-Riverol, Y., Bai, J., Bandla, C., García-Seisdedos, D., Hewapathirana, S., Kamatchinathan, S., Kundu, D.J., Prakash, A., Frericks-Zipper, A., Eisenacher, M., et al. (2022). The PRIDE database resources in 2022: a hub for mass spectrometry-based proteomics evidences. Nucleic Acids Res. *50*, D543–D552. https://doi.org/10.1093/nar/gkab1038.

53. Küspert, M., Murakawa, Y., Schäffler, K., Vanselow, J.T., Wolf, E., Juranek, S., Schlosser, A., Landthaler, M., and Fischer, U. (2015). LARP4B is an AU-rich sequence associated factor that promotes mRNA accumulation and translation. RNA *21*, 1294–1305. https://doi.org/10.1261/rna.051441.115.

54. Cox, J., and Mann, M. (2008). MaxQuant enables high peptide identification rates, individualized p.p.b.-range mass accuracies and proteome-wide protein quantification. Nat. Biotechnol. *26*, 1367–1372. https://doi.org/10.1038/nbt.1511.

55. Tyanova, S., Temu, T., and Cox, J. (2016). The MaxQuant computational platform for mass spectrometry-based shotgun proteomics. Nat. Protoc. *11*, 2301–2319. https://doi.org/10.1038/nprot.2016.136.

56. Chen, Z.L., Meng, J.M., Cao, Y., Yin, J.L., Fang, R.Q., Fan, S.B., Liu, C., Zeng, W.F., Ding, Y.H., Tan, D., et al. (2019). A high-speed search engine pLink 2 with systematic evaluation for proteome-scale identification of cross-linked peptides. Nat. Commun. *10*, 3404. https://doi.org/10.1038/s41467-019-11337-z.

57. Dobin, A., Davis, C.A., Schlesinger, F., Drenkow, J., Zaleski, C., Jha, S., Batut, P., Chaisson, M., and Gingeras, T.R. (2013). STAR: ultrafast universal RNA-seq aligner. Bioinformatics *29*, 15–21. https://doi.org/10.1093/bioinformatics/bts635.

58. Langmead, B., Trapnell, C., Pop, M., and Salzberg, S.L. (2009). Ultrafast and memory-efficient alignment of short DNA sequences to the human genome. Genome Biol. *10*, R25. https://doi.org/10.1186/gb-2009-10-3-r25.

59. Erhard, F. (2018). Estimating pseudocounts and fold changes for digital expression measurements. Bioinformatics *34*, 4054–4063. https://doi.org/10.1093/bioinformatics/bty471.

60. Erhard, F., Halenius, A., Zimmermann, C., L'Hernault, A., Kowalewski, D.J., Weekes, M.P., Stevanovic, S., Zimmer, R., and Dölken, L. (2018). Improved Ribo-seq enables identification of cryptic translation events. Nat. Methods *15*, 363–366. https://doi.org/10.1038/nmeth.4631.

61. Lorenz, R., Bernhart, S.H., Höner Zu Siederdissen, C., Tafer, H., Flamm, C., Stadler, P.F., and Hofacker, I.L. (2011). ViennaRNA Package 2.0. Algorithm Mol. Biol. *6*, 26. https://doi.org/10.1186/1748-7188-6-26.

62. Love, M.I., Huber, W., and Anders, S. (2014). Moderated estimation of fold change and dispersion for RNA-seq data with DESeq2. Genome Biol. *15*, 550. https://doi.org/10.1186/s13059-014-0550-8.

63. Rivera, M.C., Maguire, B., and Lake, J.A. (2015). Isolation of ribosomes and polysomes. Cold Spring Harb. Protoc. *2015*, 293–299. https://doi.org/10.1101/pdb.prot081331.

64. Danan, C., Manickavel, S., and Hafner, M. (2016). PAR-CLIP: A Method for Transcriptome-Wide Identification of RNA Binding Protein Interaction Sites. Methods Mol. Biol. *1358*, 153–173. https://doi.org/10.1007/978-1-4939-3067-8_10.

65. Weinberg, D.E., Shah, P., Eichhorn, S.W., Hussmann, J.A., Plotkin, J.B., and Bartel, D.P. (2016). Improved Ribosome-Footprint and mRNA Measurements Provide Insights into Dynamics and Regulation of Yeast Translation. Cell Rep. *14*, 1787–1799. https://doi.org/10.1016/j.celrep.2016.01.043.

66. Guenther, U.P., Weinberg, D.E., Zubradt, M.M., Tedeschi, F.A., Stawicki, B.N., Zagore, L.L., Brar, G.A., Licatalosi, D.D., Bartel, D.P., Weissman, J.S., and Jankowsky, E. (2018). The helicase Ded1p controls use of near-cognate translation initiation codons in 5' UTRs. Nature *559*, 130–134. https://doi.org/10.1038/s41586-018-0258-0.

67. Meyer, K., Ferraiuolo, L., Miranda, C.J., Likhite, S., McElroy, S., Renusch, S., Ditsworth, D., Lagier-Tourenne, C., Smith, R.A., Ravits, J., et al. (2014). Direct conversion of patient fibroblasts demonstrates non-cell autonomous toxicity of astrocytes to motor neurons in familial and sporadic ALS. Proc. Natl. Acad. Sci. USA *111*, 829–832. https://doi.org/10.1073/pnas.1314085111.

STAR★METHODS

KEY RESOURCES TABLE

REAGENT or RESOURCE	SOURCE	IDENTIFIER
Antibodies		
Rabbit polyclonal anti-IGHMBP2	Surrey et al.[51]	RRID: AB_3086806
Rabbit polyclonal anti-RPL7	Abcam	ab72550; RRID: AB_1270391
Rabbit monoclonal anti-RPS6	Abcam	ab225676; RRID: AB_3086804
Mouse monoclonal anti-THOC1	Santa Cruz Biotechnologies	sc136426, clone THOC1 (29); RRID: AB_10610671
Rabbit polyclonal anti-THOC2	Abcam	ab129485; RRID: AB_11154716
Rabbit polyclonal anti-THOC6	Niels Gehring, University of Cologne (unpublished)	GenScript Custom antibody, Epitope: CRERSPEVLSGGEDG
Rabbit polyclonal anti-THOC5	Niels Gehring, University of Cologne (unpublished)	GenScript Custom antibody, Epitope: KRNRSDTEQEGKYYC
Rabbit polyclonal anti-LC3B	Sigma Aldrich	L7543; RRID: AB_796155
Mouse monoclonal anti-Ubiquitin	Enzo Life Sciences	BML-PW0930-100, clone P4D1; RRID: AB_11181462
Rabbit polyclonal anti-eIF2γ (eIF2S3)	Proteintech	11162-1-AP; RRID: AB_2246331
Rabbit polyclonal anti-PXN	Sigma Aldrich	SAB4300459; RRID: AB_1062442
Rabbit polyclonal anti-CALD1	Sigma Aldrich	HPA008066; RRID: AB_1078378
Rabbit polyclonal anti-CRIP2	Sigma Aldrich	HPA042664; RRID: AB_1079701
Rabbit polyclonal anti-TGFBI	Sigma Aldrich	SAB1411345; RRID: AB_3086805
Mouse monoclonal anti-HA.11 epitope tag	BioLegend	901515, clone 16B12; RRID: AB_2565334
Mouse monoclonal anti-GAPDH	UBP Bio	Y1041, clone GA1R; RRID: AB_3086807
Mouse monoclonal anti-β-Actin	Sigma Aldrich	A5316, clone AC-74; RRID: AB_476743
Mouse monoclonal anti-α-Tubulin	Sigma Aldrich	T5168, clone B-5-1-2; RRID: AB_477579
Goat polyclonal anti-mouse IgG	Sigma Aldrich	A4416; RRID: AB_258167
Goat polyclonal anti-rabbit IgG	Sigma Aldrich	A6154; RRID: AB_258284
Bacterial and virus strains		
E. coli DH5α	New England BioLabs	C2987I
E. coli Rosetta-gami (DE3)pLysS	Sigma Aldrich	71137
AAV9.IGHMBP2	Sierra-Delgado et al.[43]	ClinicalTrials.gov: NCT05152823
Chemicals, peptides, and recombinant proteins		
3xFLAG peptide	Sigma Aldrich	F4799
Anti-FLAG M2 agarose beads	Sigma Aldrich	A2220
Glutathione Sepharose 4 fast flow beads	Merck	GE17-5132-01
Ni-NTA Superflow beads	Qiagen	30230
cOmplete, EDTA-free Protease Inhibitor Cocktail	Sigma Aldrich	4693132001
^{12}C- Lysine	Sigma Aldrich	L-8662
^{12}C- Arginine	Sigma Aldrich	A-6969
^{13}C,^{15}N – Lysine (Lys-8)	Cambridge Isotope Laboratories	CNLM-291-H
^{13}C,^{15}N – Arginine (Arg-10)	Cambridge Isotope Laboratories	CNLM-539-H
^{2}H – Lysine (Lys-4)	Cambridge Isotope Laboratories	DLM-2640
^{2}H – Arginine (Arg-6)	Cambridge Isotope Laboratories	CLM-2265-H
Tetracycline	Sigma Aldrich	87128
L-Arginine	Sigma Aldrich	A5006
L-Glutamate	Sigma Aldrich	G1626

(*Continued on next page*)

Continued

REAGENT or RESOURCE	SOURCE	IDENTIFIER
Blasticidin	Invivogen	Ant-bl-5
Zeocin	Invivogen	Ant-zn-1
Hygromycin B, Gold	Invivogen	Ant-hg-5
Murine RNase inhibitor	New England BioLabs	M0314L
BS3 (Bis(sulfosuccinimidyl)suberat)	ThermoFisher Scientific	21585
RNase T1	ThermoFisher Scientific	EN0542
FastAP Thermosensitive Alkaline Phosphatase	ThermoFisher Scientific	EF0654
T4 Polynucleotide Kinase (PNK)	ThermoFisher Scientific	EK0031
γ-^{32}P-ATP	Hartmann Analytic	SRP-501
NuPAGE Sample reducing agent	ThermoFisher Scientific	NP0004
NuPAGE MOPS SDS running buffer	ThermoFisher Scientific	NP0001
Proteinase K	Roche	03115879001
RNase I	Invitrogen	AM2294
Turbo-DNase	Invitrogen	AM2238
SUPERase·In RNase Inhibitor	Invitrogen	AM2694
MyOne Streptavidin C1 Dynabeads	Invitrogen	65001
CircLigase I	Epicenter	CL4111K
GlycoBlue	Invitrogen	AM9515
T4 Polynucleotide kinase	New England BioLabs	M0201S
T4 RNA Ligase 2, Truncated	New England BioLabs	M0242S
Superscript IV	Invitrogen	18090010
Universal miRNA cloning linker 5′	New England BioLabs	S1315S
Biotinylation subtraction oligonucleotides	Ingolia et al.,[38]	N/A
Phusion polymerase	New England BioLabs	M0530S
Yeast 5′ Deadenylase	New England BioLabs	M0331S
RecJ Exonuclease	New England BioLabs	M0264S
DMEM, high glucose and pyruvate	Gibco	41965062
FBS	Gibco	A5256701
DMEM, high glucose, no glutamine, no lysine, no arginine (for pSILAC)	Gibco	A14431-01
Dialyzed FBS (for pSILAC)	Gibco	26400036
Pencillin-Streptomycin	Gibco	15140122
Antibiotic-Antimycotic	Gibco	15240062
DMEM, high glucose, GlutaMAX Supplement, pyruvate	Gibco	10569010
DMEM/F-12, GlutaMAX supplement	Gibco	10565042
FBS (for primary cells)	Gibco	16000–036
B-27 supplement	Invitrogen	17504044
Recombinant Human FGF-basic (154 a.a.)	Preprotech	100-18B
Animal-Free Recombinant Human EGF	Preprotech	AF-100-15
Heparin	Sigma Aldrich	H3149-10KU
Neuraminidase	Sigma Aldrich	N7885
Human Plasma Fibronectin Purified Protein	Sigma Aldrich	FC010
N2-Supplement	Gibco	17502048
Universal nuclease	Pierce	88702
Nuclease P1	New England BioLabs	M0660S
Trypsin, sequencing grade modified	Promega	V511B
Spermidine	Sigma Aldrich	S2626
TRIzol	ThermoFisher Scientific	15596018
5-Fluorouracil	Sigma Aldrich	F6627

(*Continued on next page*)

Continued

REAGENT or RESOURCE	SOURCE	IDENTIFIER
Cycloheximide	Sigma Aldrich	C7698-5G
MG-132	Enzo Life Sciences	BML-PI102-0005
Bafilomycin A1	Sigma Aldrich	B1793
Critical commercial assays		
Maxima H-minus cDNA synthesis master mix with dsDNase	ThermoFisher Scientific	M1681
PowerUp SYBR Green master mix	Applied Biosystems	A25777
Turbo DNA-free kit	Invitrogen	AM1907
SENSE mRNA-Seq Library prep kit V2	Lexogen	001.24
TruSeq stranded mRNA library kit with oligo-dT capture	Illumina	20020594
NEBNext Multiplex Small RNA Library Prep Set for Illumina	New England BioLabs	E7300L
Retrovirus iPSC Reprogramming Kit	ALSTEM	RF101
Lipofectamine RNAiMAX	ThermoFisher Scientific	13778
Dual-Luciferase Reporter Assay System	Promega	E1910
In-Fusion HD Cloning Kit	Takara	639650
Deposited data		
pSILAC	This paper	ProteomeXchange Consortium via the PRIDE[52]: PXD043336
CXMS	This paper	ProteomeXchange Consortium via the PRIDE[52]: PXD044048
RNA-Seq and Ribo-Seq	This paper	GEO: GSE237412
In vitro CLIP and RIP-Seq	This paper	SRA: PRJNA996769
Mendeley data: Image files and pSILAC R-script	This paper	https://doi.org/10.17632/cnympvsrgt.4
Human reference genome NCBI build 38, GRCh38	Genome Reference Consortium	http://www.ncbi.nlm.nih.gov/projects/genome/assembly/grc/human/
Human rRNA sequences U13369.1	European Nucleotide Archive (ENA)	https://www.ebi.ac.uk/ena/browser/view/U13369.1
Human Proteome	UniProt Human Reference Proteome database	https://www.uniprot.org/proteomes/UP000005640
Experimental models: Cell lines		
HEK Flp-In T-Rex	ThermoFischer Scientific	R75007
HEK Flp-In T-Rex FLAG/HA-IGHMBP2 FL	This paper	N/A
HEK Flp-In T-Rex FLAG/HA-IGHMBP2 CT	This paper	N/A
HEK Flp-In T-Rex FLAG/HA-IGHMBP2 HD	This paper	N/A
HEK Flp-In T-Rex FLAG/HA-IGHMBP2 R3H	This paper	N/A
HEK Flp-In T-Rex FLAG/HA-IGHMBP2 ZnF	This paper	N/A
HEK Flp-In T-Rex FLAG/HA-IGHMBP2 ΔR3H	This paper	N/A
HEK Flp-In T-Rex FLAG/HA-IGHMBP2 ΔZnF	This paper	N/A
HeLa	Sigma Aldrich	93021013
HeLa S3	ATCC	CCL-2.2
Induced Astrocytes (iAs) Control, SMARD1	This paper	N/A
Human Primary Umbilical Vein Endothelial Cells (HUVEC)	ATCC	PCS-100-010
A549	ATCC	CCL-185
HEK 293	ATCC	CRL-1573
Hep G2	ATCC	HB-8065
SKOV3	Sigma Aldrich	91091004
MO3.13	Cellutions Biosystems Inc.	CLU301

(*Continued on next page*)

Continued

REAGENT or RESOURCE	SOURCE	IDENTIFIER
U251	Sigma Aldrich	09063001
Oligonucleotides		
ON-TARGETplus Human IGHMBP2 SMARTpool siRNA	Horizon Discovery	L-019657-00-0005
ON-TARGETplus Human THOC1 SMARTpool siRNA	Horizon Discovery	L-019911-00-0005
ON-TARGETplus Human THOC2 SMARTpool siRNA	Horizon Discovery	L-025006-01-0005
siGFP	Kuespert et al.[53]	Eurofins custom synthesis, Sequence: GCAAGCUGACCCUGAAGUUC
siLuciferase	Kuspert et al.[53]	Eurofins custom synthesis, Sequence: CGUACGCGGAAUACUUCGA
qPCR Primers: See Table S5	This paper	N/A
Recombinant DNA		
pRL-TK	Promega	E2241
psiCHECK-2	Promega	C8021
pcDNA3	Invitrogen	V790-20
pcDNA3-RLuc-THOC1 5′UTR-FFLuc	This paper	N/A
pcDNA3-RLuc-THOC2 5′UTR-FFLuc	This paper	N/A
pcDNA3-RLuc-Poly-U 5′UTR-FFLuc	This paper	N/A
pcDNA3-RLuc-No 5′UTR-FFLuc	This paper	N/A
pcDNA3-RLuc-Palindromic 5′UTR-FFLuc	This paper	N/A
pcDNA3-RLuc-THOC1 5′UTR-10AA THOC1- FFLuc	This paper	N/A
pcDNA3-RLuc-THOC2 5′UTR-10AA THOC2- FFLuc	This paper	N/A
pcDNA3-RLuc-THOC1 5′UTR-Myc-tag- FFLuc	This paper	N/A
pcDNA3-RLuc-THOC2 5′UTR-Myc-tag- FFLuc	This paper	N/A
pcDNA5-FRT/TO-FLAG/HA-MCS	Kuspert et al.[53]	N/A
pcDNA5-FRT/TO-FLAG/HA-IGHMBP2 FL	This paper	N/A
pcDNA5-FRT/TO-FLAG/HA-IGHMBP2 CT	This paper	N/A
pcDNA5-FRT/TO-FLAG/HA-IGHMBP2 HD	This paper	N/A
pcDNA5-FRT/TO-FLAG/HA-IGHMBP2 R3H	This paper	N/A
pcDNA5-FRT/TO-FLAG/HA-IGHMBP2 ZnF	This paper	N/A
pcDNA5-FRT/TO-FLAG/HA-IGHMBP2 ΔR3H	This paper	N/A
pcDNA5-FRT/TO-FLAG/HA-IGHMBP2 ΔZnF	This paper	N/A
pGEX-6P-1-IGHMBP2-6xHis	Guenther et al.[36]	N/A
Software and algorithms		
MaxQuant 1.6.2.2	Cox and Mann[54]	https://www.maxquant.org/
MaxQuant 1.6.17.0	Tyanova et al.[55]	https://www.maxquant.org/
pLink 2.3.11	Chen et al.[56]	http://pfind.org/software/pLink/
STAR 2.5.3a	Dobin et al.[57]	http://code.google.com/p/rna-star/
Bowtie1.2	Langmead et al.[58]	http://bowtie.cbcb.umd.edu
PsiLFC	Erhard[59]	https://github.com/erhard-lab/lfc
PRICE Version 1.0	Erhard et al.[60]	https://github.com/erhard-lab/price
ViennaRNA package Version 0.4.3	Lorenz et al.[61]	https://www.tbi.univie.ac.at/RNA/#
R Version v4.1.2	Bell Laboratories	https://www.r-project.org/
Image Lab	Biorad	https://www.bio-rad.com/de-de/product/image-lab-software?ID=KRE6P5E8Z

(*Continued on next page*)

Continued

REAGENT or RESOURCE	SOURCE	IDENTIFIER
DESeq2 Version 1.34	Love et al.[62]	http://www.bioconductor.org/packages/release/bioc/html/DESeq2.html
Other		
UV 254nm crosslinker	UVP	CL-1000S
NuPAGE 4–12% Bis-Tris gel	ThermoFisher Scientific	NP0335BOX
D-Tube Dialyzer midi MWCO 3.5kDa	Merck	71506
Vivaspin 500 MWCO 10000	Sartorius	VS0602
Superdex Peptide PC3.2/300	GE Healthcare	29-0362-31
ReproSil-Pur 120 C18-AQ, 1.9 μm pore size	Dr. Maisch GmbH	r119.aq.0001

RESOURCE AVAILABILITY

Lead contact

Further information and requests for resources and reagents should be directed to and will be fulfilled by the lead contact, Utz Fischer (utz.fischer@uni-wuerzburg.de).

Materials availability

All plasmids, unique/stable reagents generated in this study are available from the lead contact with a completed materials transfer agreement.

Data and code availability

- The mass spectrometry proteomics data have been deposited at the ProteomeXchange Consortium via the PRIDE[52] partner repository and are publicly available as of the date of publication. Accession numbers are listed in the key resources table. The RNA-seq and Ribo-seq data have been deposited to GEO and are publicly available as of the date of publication. Accession number is listed in the key resources table. The *in vitro* IGHMBP2-ribosome CLIP and resulting RIP-seq data have been submitted to SRA and are publicly available as of the date of publication. Accession number is listed in the key resources table. The raw image data have been deposited at Mendeley Data (https://data.mendeley.com/datasets/cnympvsrgt/4) and are publicly available as of the date of publication. DOI is listed in the key resources table.
- The original code (R-script) used for pSILAC data analysis has been deposited at Mendeley data (https://data.mendeley.com/datasets/cnympvsrgt/4) and is publicly available as of the date of publication. DOI is listed in the key resources table.
- Any additional information required to reanalyze the data reported in this work paper is available from the lead contact upon request.

EXPERIMENTAL MODEL AND STUDY PARTICIPANT DETAILS

All reported sex annotations in this section are based on genetic composition of the samples or sex assigned at birth. The conclusions drawn in this manuscript are not limited by the sex of the samples analyzed and can be generalized since the mechanisms studied herein are ubiquitous to cells and independent of the sex of the sample. Therefore, an SGBA was not carried out.

Cell lines

All cell lines used in this study are of human origin and acquired from commercial sources or cell banks. No additional authentication of these cells was performed during this study. HeLa (Sigma Aldrich, female), HUVEC (ATCC, female), HEK 293 (ATCC, female), A549 (ATCC, male), Hep G2 (ATCC, male), SKOV3 (Sigma Aldrich, female), MO3.13 (Cellutions Biosystems Inc, female), U251 (Sigma Aldrich, male) were grown in DMEM with high glucose and pyruvate (Gibco), supplemented with 10% FBS (Gibco) and 1% Penicillin-Streptomycin (Gibco). HEK Flp-In T-Rex (female) parent cells were grown in DMEM with high glucose and pyruvate, containing Zeocin (Invivogen) at 100 μg/mL and Blasticidin (Invivogen) at 10 μg/mL, supplemented with 10% FBS and 1% Penicillin-Streptomycin. HEK Flp-In T-Rex FLAG/HA-IGHMBP2 cells were grown in DMEM with high glucose and pyruvate, containing Hygromycin B at 100 μg/mL and Blasticidin (Invivogen) at 10 μg/mL, supplemented with 10% FBS and 1% Penicillin-Streptomycin. All adherent cells listed above were cultured in a humidified incubator maintained at 37°C and 5% CO_2. HeLa S3 (ATCC, female) was grown as a suspension culture in DMEM with 5% FBS and 1% Penicillin-Streptomycin in a 13-L capacity bioreactor at 37°C and 5% CO_2.

Primary cell cultures

Primary fibroblasts were isolated from skin biopsies from healthy individuals (#9/female, #155/male) and patients with SMARD1 disease (#4342/male, #208/female) or another neurological disease (non-SMARD1, #3459/male) at Nationwide Children's hospital as per the ethical clearance number IRB14-00719 and informed consent was obtained from all participants. Fibroblasts were cultured in fibroblast media containing DMEM with high glucose, GlutaMAX supplement and pyruvate (Gibco) supplemented with 10% FBS and 1% Antibiotic-Antimycotic (Gibco). For conversion into iNPCs, the cells were grown in conversion media containing DMEM/F12 + Glutamax supplement (Gibco), 1%N2 (Gibco), 1% B-27 (Gibco), 1% Antibiotic-Antimycotic, 20 ng/mL FGF (Preprotech), 20 ng/ml EGF (Preprotech) and 5 μg/mL Heparin (Sigma). iNPCs were grown in media containing DMEM/F12 + Glutamax supplement, 1% N2, 1% B-27, 1% Antibiotic-Antimycotic and FGF at 2 ng/mL. Astrocytes were cultured in fibroblast media with the addition of 0.2% N2. All cells were cultured in a humidified incubator maintained at 37°C and 5% CO_2.

Bacterial cells

E.coli DH5α (New England Biolabs) was grown in LB media containing respective antibiotics and Rosetta-gami (DE3)pLysS (Sigma Aldrich) were grown in SB-media with antibiotics. Both were cultured at 37°C and 180 rpm for normal exponential growth and Rosetta-gami (DE3)pLysS were cultured at 16°C and 110 rpm during protein expression and induced with 1mM IPTG at OD_{600nm} = 0.8.

METHOD DETAILS

Cell culture and RNAi-mediated knockdown

Full-length or truncated *IGHMBP2* cDNA sequence was cloned into FRT/TO-Flag/HA vector[53] and stably transfected into HEK293 Flp-In T-Rex cells (Thermofisher Scientific) and induced with 0.5 μg/mL tetracycline for 6 h prior to cell pelleting. Knockdown of IGHMBP2 was carried out using ON-TARGETplus Human IGHMBP2 SMARTpool siRNA (Horizon discovery) at 50 pmol siRNA per well in a 6-well plate for 72 h (pSILAC, Ribo-seq and RNA-seq data) or 96 h (for comparison with THOC knockdown RNA-seq). Control cells were transfected with siRNA against luciferase or GFP at the same concentration as other specific knockdowns. siGFP control siRNA was used only in luciferase assay experiments. In all other experiments, control knockdowns were performed using the siRNA against luciferase. Knockdown of THOC1 and THOC2 were carried out using ON-TARGETplus Human THOC1 and THOC2 SMARTpool siRNAs, respectively, (Horizon discovery) at 50 pmol siRNA per well in a 6-well plate for 96 h siRNA transfections were carried out using Lipofectamine RNAiMAX (ThermoFisher Scientific) as per manufacturer's protocol using 4 μL Lipofectamine RNAiMAX per transfection.

Mono/polysome density gradient centrifugation

HEK 293 Flp-In T-Rex cells were induced for exogenous expression of FLAG/HA-IGHMBP2 (full-length or truncated) as described above. Cells were then treated with 100 μg/mL cycloheximide for 20 min prior to pelleting to arrest translating ribosomes, cells were washed with ice-cold 1xPBS containing 100 μg/mL cycloheximide prior to resuspension in lysis buffer (20 mM HEPES-KOH pH 7.5, 100 mM KCl, 5 mM $MgCl_2$, 0.5% NP40, 100 μg/mL cycloheximide, 4 U/ml murine RNase inhibitor and protease inhibitor cocktail). Lysates were cleared by centrifugation at 10000*g* for 10 min. The supernatants were then analyzed using 5–45% w/v sucrose density gradient centrifugation at 34500 rpm for 2 h in SW41Ti rotor (Beckman Coulter) for monosome and polysome interaction. To analyze only 40S, 60S and monosome interaction, the lysates were layered on a 5–30% sucrose density gradient and centrifuged at 38000rpm for 4 h in SW41Ti rotor. The fractions were collected using a Biocomp gradient harvester and analyzed by SDS-PAGE and Western blotting.

Purification of recombinant IGHMBP2

Full-length IGHMBP2 was recombinantly expressed using pGEX-6P-1-*IGHMBP2*-6xHis in Rosetta-gami (DE3)pLysS cells as previously described.[36] Briefly, large scale bacterial cultures were grown at 37°C in SB-media with 2% Glucose containing ampicillin and protein expression was induced using 1mM IPTG in the presence of 2% ethanol at 16°C for 16 h once the culture reached an OD_{600nm} of 0.8. Cells were pelleted at 4000 rpm for 15 min in JS 4.2 rotor (Beckman Coulter) and resuspended in lysis buffer (20 mM HEPES pH 7.5, 500 mM NaCl, 5 mM $MgCl_2$, 10% glycerol, 0.01% NP40, 50 mM arginine, 5 mM β-mercaptoethanol, 1:1000 protease inhibitor cocktail) and lysed on ice by sonication. After centrifugation at 25000 rpm for 1 h at 4°C in 45Ti rotor (Beckman Coulter), the lysate was incubated with Glutathione Sepharose beads (Merck) for 2 h at 4°C on a head-over-tail rotor. The beads were then washed with 50 column volumes (CV) of lysis buffer and 50 CV of wash buffer I (20 mM HEPES pH 7.5, 500 mM NaCl, 5 mM $MgCl_2$, 10% glycerol, 10 mM imidazole, 50 mM arginine, 5mM β-mercaptoethanol) and eluted with 3 column volumes of elution buffer I (wash buffer I with 50mM reduced glutathione). This eluate was incubated with Ni-NTA superflow beads (Qiagen) for 2 h at 4°C on a head-over-tail rotor. After washing with 100 CV of wash buffer I, and 100 CV wash buffer II (20 mM HEPES pH 7.5, 100 mM NaCl, 5 mM $MgCl_2$, 10% glycerol, 10 mM imidazole, 50 mM arginine, 5 mM β-mercaptoethanol), the bound protein was eluted with 4CV of elution buffer II (wash buffer II containing 300mM imidazole).

Purification of 80S ribosomes

Ribosomes were purified from HeLa S3 cells.[63] Briefly, HeLa S3 cell pellets were resuspended in 3 pellet volumes of hypotonic lysis buffer (20 mM HEPES pH 7.5, 10 mM KAc, 5 mM MgAc, 2 mM DTT, 1:1000 protease inhibitor cocktail). After incubation on ice for

10 min, cells were lysed using Dounce homogenizer. Cell debris were removed by centrifugation at 23000*g* for 30 min at 4°C in JA 25.50 rotor (Beckman Coulter). 15 mL of this supernatant was layered on 50 mL sucrose cushion (1M sucrose, 20 mM HEPES pH 7.5, 100 mM KAc, 5 mM MgAc, 2 mM DTT) and centrifuged at 40000 rpm for 4 h at 4°C in 45Ti rotor (Beckman Coulter). The crude ribosomal pellet was washed with 7 mL high salt resuspension buffer I (20 mM HEPES pH 7.5, 500 mM KAc, 5 mM MgAc, 2 mM DTT) and resuspended in 2 mL of the same buffer on an orbital shaker at 120 rpm for 16 h. The crude ribosomes were loaded on a 50 mL high salt sucrose cushion (1 M sucrose in resuspension buffer I) and centrifuged at 40000 rpm for 4 h at 4°C in 45Ti rotor. The pellet was again resuspended and subjected to gradient centrifugation in 10–30% sucrose in resuspension buffer I at 22000 rpm, for 12 h at 4°C using SW32 rotor (Beckman Coulter). The gradient was harvested in 2 mL fractions, and the RNA content of each fraction was measured using absorbance at 260 nm using a spectrophotometer. 80S peak fractions were pooled and pelleted at 40000 rpm for 4 h at 4°C in 45Ti rotor. This 80S pellet was then washed with 7 mL resuspension buffer II (20 mM HEPES pH 7.5, 100 mM KAc, 5 mM MgAc, 2 mM DTT) and resuspended in 2 mL of the same. 80S concentration was determined by RNA measurement. Aliquots were frozen in liquid nitrogen and stored at −80°C.

In vitro IGHMBP2-ribosome CLIP

Purified recombinant GST-IGHMBP2-His_6 was dialyzed twice for 2 h at 4°C against elution buffer without imidazol (20 mM HEPES pH 7.5, 500 mM NaCl, 10% glycerol, 50 mM arginine, 50 mM glutamate, 5 mM β-mercaptoethanol). Recombinant IGHMBP2 and 80S ribosomal particles were mixed in a 1:1 M ratio, incubated for 10 min on ice, followed by an incubation at 30°C for 10 min and another incubation for 15 min on ice. The IGHMBP2-80S sample was loaded on a 10–30% sucrose gradient (20 mM HEPES pH 7.5, 100 mM KAc, 6 mM MgAc, 2 mM DTT) and centrifuged at 38000 rpm for 90 min at 4°C in a SW60Ti rotor (Beckman Coulter). Gradient fractions were harvested, and the peak fractions pooled for crosslinking. Samples were crosslinked twice under UV_{254nm} (UVP) at 240 mJ/cm^2 and treated with RNase T1 at 1 U/μl (ThermoFisher Scientific) for 7 min at 22°C and then incubated for 5 min on ice.

The protocol for identification of RNA interactors was adapted from an established PAR-CLIP protocol.[64] After binding to Glutathione Sepharose beads for 1 h at 4°C on a head-over-tail rotor and washing the beads thrice with IP-buffer (50 mM HEPES pH 7.5, 300 mM KCl, 0.05% NP40, 0.5 mM DTT, 1:1.000 protease inhibitor cocktail), the second RNase T1 treatment (100U/μL) was carried out for 15 min at 22°C. Samples were incubated for 5 min on ice. The beads were then washed thrice with high salt buffer (50 mM HEPES pH 7.5, 500 mM KCl, 0.05% NP40, 0.5 mM DTT, 1:1.000 protease inhibitor cocktail) and twice with FastAP buffer (10 mM Tris-HCl pH 8.0 at 37°C, 5 mM MgCl2, 100 mM KCl, 0.02% Triton X-100 and 0.1 mg/mL BSA). The bound RNA was dephosphorylated using 0.15 U/μl FastAP (ThermoFisher Scientific) for 30 min at 37°C on a shaker at 800 rpm. Beads were then washed twice with FastAP buffer and twice with T4-PNK buffer A (50 mM Tris-HCl pH 7.6 at 25°C, 10 mM MgCl2, 5 mM DTT, 0.1 mM spermidine). Radiolabeling of interacting RNA was done using 0.5 μCi/μL γ-^{32}P-ATP (Hartmann Analytic) and 1 U/μL T4-PNK (ThermoFisher Scientific) for 30 min at 37°C. The beads were washed five times with T4-PNK buffer A. The beads were then denatured in 1x NuPAGE sample reducing agent (ThermoFisher Scientific) and separated on a NuPAGE 4–12% Bis-Tris gel (ThermoFisher Scientific). Following autoradiography of the gel, the part of the gel corresponding to GST-IGHMBP2-His_6 was cut, placed in a D-Tube Dialyzer midi MWCO 3.5kDa tube (Merck) and electroeluted on ice in NuPAGE MOPS SDS running buffer (ThermoFisher Scientific) for 2 h at 100 V and for 2 min with reverse voltage. The eluate was transferred to siliconized tubes and treated with Proteinase K (Roche) in Proteinase K buffer (50 mM Tris pH 8.0, 3 mM $CaCl_2$, 50% glycerol) for 60 min at 55°C. Following phenol-chloroform extraction, the RNA was precipitated using 1 mL ethanol containing 30 μL NaCl (3M) and 1 μL GlycoBlue (ThermoFisher Scientific) at −20°C for 16 h. The precipitate was washed twice with 80% ethanol and resuspended in nuclease-free water. NEB Next Multiplex Small RNA Library Prep Set for Illumina was used for 3′ and 5′ adapter ligation and library preparation as per manufacturer's instructions.

Pulsed-SILAC labeling and mass spectrometry

Control and IGHMBP2 siRNA transfected cells were grown in lysine and arginine-free DMEM media (Gibco) containing 10% dialyzed FBS (Gibco) and light amino acids for 48 h after transfection (Sigma, L-^{12}C-Lysine and ^{12}C-Arginine). Then the control cells were grown in DMEM containing heavy isotope amino acids (Cambridge Isotope Laboratories, ^{13}C, ^{15}N-Lysine/Lys-8 and ^{13}C, ^{15}N-Arginine/Arg-10) whereas the IGHMBP2 knockdown cells were grown in medium heavy amino acids (Cambridge Isotope Laboratories, ^{2}H-Lysine/Lys-4 and ^{13}C-Arginine/Arg-6) for 24 h. Following this, cells were lysed and processed by mass spectrometry as previously described.[53] Raw MS data files were analyzed with MaxQuant version 1.6.2.2.[54] Database search was performed with Andromeda, which is integrated in the utilized version of MaxQuant. The search was performed against the UniProt Human Reference Proteome database (June 2022, UP000005640, 79684 entries). Additionally, a database containing common contaminants was used. The search was performed with tryptic cleavage specificity with 3 allowed miscleavages. Protein identification was under control of the false-discovery rate (FDR; <1% FDR on protein and peptide spectrum match (PSM) level). In addition to MaxQuant default settings, the search was performed against following variable modifications: Protein N-terminal acetylation, Gln to pyro-Glu formation (N-term. Gln) and oxidation (Met). Carbamidomethyl (Cys) was set as fixed modification. Arg6 and Lys4 were set for medium SILAC labels and Arg10 and Lys8 for heavy SILAC labels (control). Further data analysis was performed using R scripts developed in-house. For quantification of pSILAC-labeled proteins, the median was calculated from log2-transformed normalized peptide medium-to-heavy ratios (M/H) for each protein. Two ratio counts were required for protein quantification. The median M/H protein ratio was calculated from two replicates. Outliers were identified in intensity bins of at least 300 proteins per bin by boxplot statistics as significantly altered if their values were outside a 1.5x interquartile range (IQR) (sig. 2, outliers) or 3x IQR (sig. 3, extreme outliers).

Purification of FLAG/HA-IGHMBP2-ribosomes

HEK 293 Flp-In T-Rex cells were induced for exogenous expression of FLAG/HA-IGHMBP2 (full-length) as described above. After washing with cold PBS, cells were resuspended in lysis buffer (50 mM HEPES pH 7.5, 150 mM NaCl, 3 mM MgCl2, 0.5% NP40, 10% glycerol, 0.5 mM DTT, 4 U/ml RNase inhibitor and protease inhibitor cocktail). After centrifugation at 11000*g* for 20 min at 4°C, the supernatant was incubated with anti-FLAG M2 agarose beads (Sigma-Aldrich) for 2 h at 4°C on a head-over-tail rotor. After five washes with lysis buffer, the IGHMBP2 protein complexes were eluted with 1CV elution buffer (lysis buffer containing 200 μg/mL 3xFLAG peptide (Sigma-Aldrich) for 16 h at 4°C on a head-over-tail rotor. The eluate was subjected to 10–45% sucrose density gradient centrifugation at 34500 rpm for 2 h using SW60Ti rotor (Beckman Coulter). The gradient was harvested by hand and the proteins were analyzed by 12% Bis-Tris SDS-PAGE. The fractions containing the IGHMBP2/ribosome complexes were pooled and concentrated using Vivaspin 500, MWCO 10000 concentrator (Sartorius). Sucrose in the pooled fractions were diluted out using buffer exchange during concentration and then used for BS3 cross-linking.

IGHMBP2-80S BS3 cross-linking and CXMS

100 μg purified human 80S ribosome-IGHMBP2 complexes were crosslinked with 2 mM BS3 (ThermoFisher Scientific) for 1 h at room temperature, quenched with 50 mM Tris-HCl, pH 7.5, and precipitated with ethanol. After centrifugation, the pelleted complexes were washed with 80% ethanol and dried. Subsequently, the complexes were dissolved in 4 M Urea/50 mM ammonium bicarbonate buffer, reduced with 10 mM DTT for 45 min at RT, acetylated with 40 mM iodoacetamide for 30 min at RT in the dark and diluted with 50 mM ammonium bicarbonate buffer to 1 M Urea. RNA was digested with 1 μL Universal nuclease (Pierce) and 1 μL Nuclease P1 (New England Biolabs) for 2 h at 37°C, followed by an overnight digestion of proteins using 5 μg trypsin (Promega) at 37°C. The sample was acidified with formic acid (FA) to an end concentration of 0.1% (v/v) and acetonitrile (ACN) was added to 5% (v/v). Peptides were reversed-phase extracted with Micro SpinColumns C18 (Harvard Apparatus), dissolved in 30% (v/v) ACN/0.1% TFA (v/v) and fractionated by size-exclusion chromatography (pSEC) on an Agilent 1200 Series HPLC system using a Superdex Peptide PC3.2/300 column (GE Healthcare) at a flow rate of 50 μL/min. One-minute-fractions containing the crosslinked peptides were vacuum dried and dissolved in 5% ACN/0.1% TFA for a subsequent uHPLC-ESI-MS/MS analysis. Online chromatographic separation was performed using a Dionex Ultimate 3000 UHPLC (Thermo Fischer Scientific) equipped with a custom 30 cm C18 column (75 μm inner diameter, packed with ReproSil-Pur 120 C18-AQ, 1.9 μm pore size, Dr. Maisch GmbH). Flow rate was set to 300 nL/min and 45 min linear gradient was formed with mobile phase A (0.1% v/v FA) and B (80% ACN, 0.08% FA) from 10%, 15 or 20%–46% mobile phase B for early, intermediate and late pSEC fractions, respectively. Data were acquired in a Q Exactive HF-X mass spectrometer (ThermoFischer Scientific) in technical duplicates. Resolution for MS1 scans was set to 120 000, automatic gain control target to 1e6 and dynamic exclusion to 30 s. Top30 precursors with a charge of 3–8 were isolated with 1.4 m/z window and fragmented with normalized collision energy of 30. MS2 spectra were acquired at resolution of 30 000, maximum injection time of 128 ms and automatic gain control target of 2e5.

CXMS data analysis

Proteins present in the human 80S ribosome-IGHMBP2 complexes were identified by MaxQuant 1.6.17.0[55] in a search against a database containing human proteome (UniProt database of main protein isoforms), common contaminants and a sequence of FLAG/HA-tagged IGHMBP2. The proteins identified were used to compile a database for a subsequent search of protein-protein crosslinks with pLink 2.3.11 (http://pfind.org/software/pLink/).[56]

RNA extraction and RT-qPCR

Control, IGHMBP2, THOC1, THOC2 and THOC1+2 knockdown cells were resuspended in TRIzol (ThermoFisher Scientific) and RNA extracted as per manufacturer's protocol. 3 μg of this RNA was used for cDNA synthesis using Maxima H-minus cDNA synthesis master mix with dsDNase (Thermofisher Scientific) as per manufacturer's protocol. RT-qPCR of the different targets was performed using primers listed in Table S5 and PowerUp SYBR Green master mix (Applied Biosystems) in QuantStudio5 real-time PCR system. Exosome inhibition was achieved by treating cells with 40 μM 5-fluorouracil (5-FU) for 24 h prior to cell lysis and RNA extraction.

RNA-seq, Ribo-seq and data processing

RNA samples for sequencing were treated with Turbo DNA-free kit (Invitrogen) and RNA quality controlled on a Bioanalyzer. Libraries were prepared from these RNA samples using SENSE mRNA-seq Library Prep Kit V2 (Lexogen) or TruSeq stranded mRNA library kit with oligo-dT capture (Illumina) and sequenced by NextSeq 500 platform with high-output (~400 M pairs). For RNA-seq after control or IGHMBP2 knockdown (72 h), we used single end single-end 1 x 75 bp (75 cycles) and for RNA-seq after control or THOC or IGHMBP2 knockdowns (96 h), we used paired-end 2 x 75bp (150 cycles) sequencing. For Ribo-seq, the control and IGHMBP2 knockdown cells were briefly trypsinized after 72 h of siRNA transfection and pelleted. The cells were washed with ice-cold PBS and snap frozen prior to analysis. The cells were resuspended in polysome buffer as previously described and processed for Ribo-seq.[38,65] Briefly, cells were thawed on ice and cold ribosome lysis buffer was added. Cells were lysed by pushing the lysate 12 times through a 25 G sized needle. The lysate was then pre-cleared by centrifugation using a tabletop centrifuge at 850xg for 2 min. The supernatant was transferred to a new tube and further spun at 18000 rpm for 5 min at 4°C. The supernatant containing the cleared lysate was again transferred to a new tube and [1% final conc] Triton X-100 was added. 2 μL RNase I (Invitrogen) and 4 μL

Turbo-DNase (Invitrogen) was added to 20 A_{260} units of total cell extract and incubated for 15 min at 25°C. Nuclease treatment was stopped by addition of 12 μL SUPERase•In RNase inhibitor (Invitrogen) and placing tubes on ice. Nuclease-treated extract was then added on top of a 15–45% sucrose gradient. Gradients were centrifuged in a SW40Ti rotor (Beckman Coulter) at 40000 rpm for 162 min at 4°C. The gradient was subsequently fractionated and fractions containing the monosomes were collected. Two volumes of 100% ethanol was added to each fraction tube and RNA was precipitated overnight at −80°C. Purification and processing of ribosome-protected fragments (RPFs) were carried out exactly as described.[66] rRNA depletion was performed at the level of circularized cDNA as described[38] with 1 μL of a 5 μM mix of biotinylated DNA oligos and MyOne Streptavidin C1 DynaBeads (Invitrogen). PCR amplification was performed as described.[66] Sizing, concentration and quality of each final DNA library was assessed on an Agilent 2100 Bioanalyzer system. DNA libraries were pooled before performing 75 bp single-end read sequencing on an Illumina NextSeq 500 platform.

We mapped all RNA-seq reads against the human genome (Ensembl v90) using STAR 2.5.3a[57] with standard parameters. We computed log2 fold changes using PsiLFC.[59] For Ribo-seq processing, reads were mapped against human rRNA sequences (U13369.1) using bowtie 1.2[58] with parameters "-a -m 100 -v 3 –best –strata –norc" and discarded all mapped reads. Then, all remaining reads were mapped against the human genome and transcriptome (Ensembl v90) using bowtie with parameters "with parameters -a -m 100 -v 3 –best –strata" (genome) or "with parameters -a -m 100 -v 3 –best –strata –norc" (transcriptome). Genomic and transcriptomic mappings were merged by transferring all transcriptomic mappings to the genome via the genomic coordinates of the annotated transcripts and only retaining all mappings with minimal number of mismatches for each read. We then used Price version 1.0[60] with parameters "-percond -plot" to identify and quantify translated codons. Then, for each gene, we determined the total read count in the coding sequence across all libraries for each isoform and identified the isoform with maximal number of mapped reads (max-isoform). Based on this, we defined the major isoform to be the one with maximal read coverage (total number of reads divided by coding sequence length) among all isoforms with a total read count exceeding 90% of the max-isoform. This major isoform and its profile of codons quantified by Price was then used for all subsequent analyses. We computed log2 fold changes using PsiLFC,[59] and TE by subtracting the RNA-seq log2 fold change from the Ribo-seq log2 fold change. We computed the start codon stalling (SCS) score for a gene as the log2 fold change[59] siIGHMBP2 vs. siControl by using the total count of codons 4–12 across both replicates, respectively. We defined genes with score<−1 to have strong SCS, with −1<score<0 to have weak SCS, and with score>0 to have no SCS. To compute the upstream folding energy, we extracted the sequences 60 nucleotides upstream of the start codon for each gene and used RNAfold from the Vienna RNA package version 0.4.3[61] to compute the minimum free energy of each of these sequences.

For the analysis of the RNA-seq data involving THO complex knockdowns, we used DESeq2 version 1.34.[62] Three samples were identified as outliers in a principal component analysis (replicate 2 of siControl, replicate 3 of siIGHMBP2, and replicate 1 of siTHOC2) and were excluded from subsequent analyses. The genes shown in Figure 3C were determined by a Wald test comparing siTHOC1+2 vs. siControl (Benjamini-Hochberg corrected p value < 1%). Shown as colors are log fold changes computed as the differences of the regularized log (rlog from DESeq2) expression values to the average rlog value of siControl. The correlation coefficients were computed using the cor function of R version v4.1.2 after averaging the rlog values across replicates.

Dual-luciferase vectors and luciferase assay

We altered the MCS of the pcDNA3 vector to introduce a Kpn1 site at the 5′end of the MCS, immediately downstream of the CMV promoter using in-fusion HD cloning (Takara Bio). Renilla luciferase coding sequence along with HSV-TK promoter and SV40 polyA sequence was amplified from pRL-TK vector and cloned into pcDNA3 vector using in-fusion HD cloning. THOC1 and THOC2 as well as the poly-U 5′UTRs were introduced during PCR amplification of firefly luciferase from psiCHECK-2 vector and cloned immediately downstream of the CMV promoter using in-fusion HD cloning to avoid introduction of additional bases between the CMV promoter and the 5′UTR sequence. For MCS as control 5′UTR, the firefly sequence was cloned using XhoI, located toward the 3′end of the pcDNA3 MCS. Control and IGHMBP2 knockdown cells (72 h of knockdown) were transfected with the dual-luciferase plasmid 24 h prior to lysis for luciferase assay. Luciferase assay was performed using dual-luciferase reporter assay system (Promega) as per manufacturer's protocol, using TriStar LB 941 Luminometer (Berthold Technologies).

Primary fibroblasts and induced astrocytes

Primary fibroblasts were isolated from skin biopsies collected from healthy individuals and patients with SMARD1 disease at Nationwide Children's hospital as per the ethical clearance number IRB14-00719 and informed consent was obtained from all participants. Cultured primary fibroblasts converted to induced neuronal precursors and then to induced astrocytes as previously described.[40,67] Briefly, 100,000–200,000 fibroblasts were seeded in a well of a 6-well plate and on the next day transduced with four retroviral vectors containing the Yamanaka reprogramming factors Oct3/4, Sox2, Klf4, and c-Myc (ALSTEM), and then the medium was changed 24 h post-infection. Two days post-transduction, the fibroblast medium was replaced by conversion medium containing FGF (Preprotech), EGF (Preprotech) and Heparin (Sigma Aldrich) for approximately 5–7 days. The cells were closely observed every day and transferred as necessary to new wells. Once the cell morphology changed and iNPC growth became obvious and persisted, the medium was switched to iNPC medium containing only FGF. After conversion of the fibroblasts to iNPCs, the iNPCs were frozen down in exact portions to thaw directly in 1 well of a 6-well plate to start astrocyte differentiation. iNPCs were seeded in medium containing 10% FBS and 0.2% N2 supplement (Gibco) and astrocytes were allowed to mature for a week. For AAV9.IGHMBP2 treatment, a

modified version of previously published protocols was used.[43] Briefly, iNPC portions were thawed and then treated with neuraminidase (Sigma Aldrich) for 2 h. Then iAs were transduced with AAV9.IGHMBP2 at a Multiplicity of Infection of 100,000K. After adding the virus, iAs conversion continued according to the previously described methodology. After the treatments, the cells were resuspended in 1x SDS-loading dye and analyzed by SDS-PAGE followed by western blotting.

QUANTIFICATION AND STATISTICAL ANALYSIS

'n' refers to the number of independent biological replicates, unless otherwise stated. For individual cases the exact number of replicates is described in the figure legend. All Western blots were quantified using Image Lab (Biorad). For Western blots and RT-qPCR analysis, the bar graphs represent the mean of the different replicates, the error bar represents the standard error of mean (SEM) and p values were calculated using Student's t-test using Microsoft Excel. The statistical analysis for RNA-seq and Ribo-seq were carried out using two-sided Kolmogorov-Smirnov test and two-sided binomial test as specified in the STAR methods section.